

# Far from equilibrium phase transition induced by solid-state reaction in the Fe–Si system

E. Gaffet, N. Malhouroux and M. Abdellaoui

Centre d'Etudes de Chimie Métallurgique-C.N.R.S., 15 Rue G. Urbain, F94407 Vitry sur Seine Cedex (France)

(Received December 2, 1991; in final form June 1, 1992)

## Abstract

In the first part of this paper, this special issue gives us the opportunity to overview systems which have been mechanically synthesized. In the second part, we report on the far from equilibrium phase transitions induced by mechanical alloying and post-milling isothermal annealing in the Fe–Si system. The end-product structures were characterized using X-ray diffraction patterns. Specific attention was paid to two particular phases exhibiting some very interesting physical properties: Fe(Si) (a crystalline phase exhibiting a magnetic effect) in which extension of the solubility limit of silicon of the crystalline Fe(Si) phase (up to 16 wt.% silicon) was observed, and  $\beta$ -FeSi<sub>2</sub> (a semiconductor-type phase exhibiting a direct optical gap and a thermoelectric power) crystalline phases.

## 1. Introduction

The crystalline to amorphous phase transition induced by ball-milling was first reported by Yermakov *et al.* [1] and Koch *et al.* [2] for the Co–Y and Ni–Nb systems respectively. This method of synthesis was previously used by Benjamin and coworkers to obtain dispersion strengthened alloys [3–7]. Subsequently, this amorphization process has been observed in many other alloy systems starting from the elemental crystalline powders and/or from a mixture of the intermetallic compounds. To our knowledge, there is no extensive summary in tabular form of such a large body of work to be found in the literature. In the context of this special issue of *The Journal of Alloys and Compounds*, such an overview is useful. Table 1 lists the various systems which have been synthesized by various mechanical methods. The crystalline to amorphous phase transition occurring in powders due to mechanical alloying (MA) was assumed to require certain conditions: a negative heat of mixing and the presence of a fast diffuser. Such a phase transition was claimed to be analogous with amorphization by solid state diffusion in multilayer systems such as Au(La, Ti, Y, Zr), Co(Sn, Zr), Cr–Ti, Fe–Zr, Ni(Ce, Si, Ti, Zr), Si–Ti (for a review see refs. 158–160). Nevertheless, MA amorphization was reported for the V–Zr [73, 148] system for which no fast diffuser is known. Recently, the crystalline to amorphous phase MA transition was reported for binary systems exhibiting a positive heat of mixing: Si–Sn [157], Si–Zn [157],

Cu–W [86], Cu–V [85], Cu–Ta [43, 74, 80, 81]. In our previous works, we reported on amorphization induced by milling of diamond cubic phases such as pure silicon [155], pure germanium [99], GaAs [38] and Ge<sub>1-x</sub>Si<sub>x</sub> [52, 103] phases. This crystalline to amorphous phase transition was attributed to instability in the crystalline lattice in relation to a decrease in grain size of the diamond cubic phase, leading to expansion of the crystalline lattice.

Another interesting point is the specific power which is injected into materials under mechanical straining (ball-milling) or irradiation conditions [161]. According to the just reported work, the injected power ranges from  $10^{-8}$  to  $10^{-2}$  eV s<sup>-1</sup> per atom, leading to an analogy between the phase transitions induced by irradiation ( $10^{-10}$ – $10^{-1}$  eV s<sup>-1</sup> per atom) and those induced by ball-milling.

In addition, attention should be given to the milling parameters which will determine the structure of the end-product, *i.e.* the energy and the frequency of the shocks as well as the mean temperature of the milling container. Indeed, a crystalline to amorphous phase transition ( $E, V, T$ ) parameter window has been revealed by recent papers [135]. This so-called window should be compared with the temperature window allowing solid state amorphization induced by diffusion [158]. In spite of the large number of alloys which have been tested (according to the papers listed in Table 1), the mechanisms leading to the phase transition under mechanical straining (mechanical alloying, ball-milling, cold

TABLE 1. Overview of the alloy systems on which the mechanical processes have been performed  
 T1, Mechanical solicitation: A attritor, C comminution, CR cold rolling, G grinding, P planetary, SBM special ball milling apparatus, SM Spex mill, V vibrating, RM rod milling, R rotating ball mill.

T2, Ball material: St steel, St\* steel or WC, St\*\* steel and/or CuBe, Aga Agate, Cer ceramic, CB Cu-Be, T3, Vial material (see T2).

T4, Protective atmosphere: Ar argon, Ar\* argon and/or air, Ar\*\* argon and/or N<sub>2</sub>, Vac vacuum.

T5, Ball-to-powder ratio or powder weight (in grams).

T6, Initial state, the subscripts denote nominal atomic percentages of the respective components: EF elemental foil, EP elemental powder, IC intermetallic compound, ICM intermetallic compound mixture, A-B\* system exhibiting a positive heat of mixing.

T7, Investigated parameters: Δt milling duration, E shock energy, ν shock frequency, E<sub>v</sub> coupled energy and frequency.

T8, Investigated composition range: crystal crystalline, am amorphous.

T9, End-product state: ms metastable, ESS extended solid solution, am amorphous phase, cryst crystalline phase, N-cryst nanocrystalline phase.

T10, Investigation methods: XRD X-ray diffraction, DSC differential scanning calorimetry, SEM scanning electron microscopy, TEM transmission electron microscopy, Mössb, DTA differential thermal analysis, TGA thermogravimetric analysis, EDX energy-dispersive X-ray analysis, EM electron microscopy, Mech, Magn, BSM, ultrason, Neutrs EXAFS, EXAFS extended X-ray absorption fine structure, neutron, RBS Rutherford backscattering spectrometry, HREM high resolution electron microscopy, Auger Auger electron spectroscopy, EPMA electron probe microanalysis.

A-B	T1	T2	T3	T4	T5	T6	T7	T8	T9	T10	References
Ag-Cu	SM	St(12.5) 1St(60)	St WC	Ar*	6	EP	Δt	Ag <sub>50</sub> Cu <sub>50</sub> Ag <sub>50</sub> La <sub>30</sub> Ag <sub>5</sub> La <sub>95</sub> Ag-56.3Fe	Am (72 h) β-La+Ag	XRD, DSC XRD	8 9, 10
Ag-Fe*	St	St	St	Ar	90	EP	—	F.c.c. Ag(Fe)+b.c.c. Fe(Ag) (600 h)	XRD, SEM, TEM, Mössb	11	
Al <sub>2</sub> O <sub>3</sub> + Fe <sub>2</sub> O <sub>3</sub>	P	—	Ag <sub>a</sub>	Air	—	—	Hydrated alumina	XRD, DTA, TGA	12		
Al-Cu	P	St	St	Ar	15	EP	Δt E <sub>v</sub>	(15-25)Cu +(10-20)Mn Al+CuO	XRD, DSC	13, 14	
-Mn	SM	3St(8g) 6St(20)	St	Ar	3	—	—	40 ≤ Al ≤ 50 50 ≤ Al ≤ 80 80 ≤ Al ≤ 90 Fe ≤ 10 17 ≤ Fe ≤ 33 Fe = 20, 24.4, 33 Al = 75.5, 80	SEM-EDX XRD, TEM, Mössb	15 16	
Al-CuO	P	—	—	Ar	90	EP	—	Cu + Al <sub>2</sub> O <sub>3</sub> N-cryst (180 h) Am (180 h) N-cryst (180 h) F.c.c. Al(Fe) Am (454 h) Am (30 passes) Am (180 h)	XRD, DSC, TEM, Mössb	17	
Al-Fe	—	—	—	Ar	90	EP	—	Fe ≤ 10 17 ≤ Fe ≤ 33 Fe = 20, 24.4, 33 Al = 75.5, 80	XRD, DSC, TEM, Mössb	17	
Al-Fe	CR	St	St	Ar	90	EP	Δt	Am (30 passes)	XRD, DSC	17	
Al-Fe	—	—	—	—	—	—	—	Am (180 h)	XRD, DSC, EM, Mössb	11, 18	
Al-Fe-Ti	—	—	—	—	—	—	—	Al-40Fe-4Ti	XRD, TEM, Mössb	11	
AlCFeO	P	St	—	—	4	EP	Δt	AlFe <sub>0.5</sub> +0.5w <sub>t</sub> C AlI <sub>3.1</sub> w <sub>t</sub> + AlMg4.2w <sub>t</sub>	XRD, SEM, TEM	19	
AlMgLi	—	—	—	—	—	—	—	Al <sub>50</sub> Nb <sub>50</sub> Al <sub>60</sub> Nb <sub>40</sub> ≥ 70 at.% Al	Hardness, DSC, TEM	20	
Al-Nb	P	—	—	—	—	EP	—	AlNb <sub>3</sub> +AlNb <sub>2</sub> Al <sub>25</sub> Nb <sub>75</sub>	XRD, DSC, TEM	21	
Al-Nb	P	St	St	Ar	10	ICM EP	—	Ms N-cryst b.c.c. (200 h)	XRD	22, 23	

Al-Ni Al-Ni	SM SM	— —	St Ar	— —	EP IC	— $\Delta t$	Al <sub>50</sub> Ni <sub>50</sub> Ni <sub>3</sub> Al	IC AlNi (30 h) Am + cryst (50 h)	XRD, DSC XRD, DSC, TEM, Hardness	24 25, 26
AlFeO Al-Pd	P SBM	— —	Aga St	Air He	— —	OxM EP	Al <sub>2</sub> O <sub>3</sub> +Fe <sub>2</sub> O <sub>3</sub> Al <sub>50</sub> Pd <sub>50</sub>	$\alpha$ -Fe <sub>2</sub> O <sub>3</sub> (+ anneal) N-cryst AlPd $\geq 66$ h	XRD, DTA, XRD, DSC	12 27
Al-Pt	WC	—	St	Ar	—	EF	Al <sub>66</sub> Pt <sub>34</sub>	Am (130 Passes)	XRD, DSC, SEM	28
Al-Ru	SM	4St St(14-19)	St	Ar	—	IC	AlRu	Cryst (32 HBM)	XRD, DSC, TEM	29, 30
Al-Ta	RM	—	St	Ar	108	EP	10 $\leq$ Al $\leq$ 70 Am (300 h)	Am + cryst Al (300 h)	XRD, DTA, SEM	31, 32
Al-Ti	SM	—	St*	Ar	—	EP	— Al <sub>2</sub> Ti <sub>55</sub> Al <sub>75</sub> Ti <sub>25</sub>	Am (9 h) Cryst Al(Ti) (21 h)	XRD, DSC	24, 33, 34
Al-Ti Al-Ti	P —	St —	St —	Ar —	8 —	EP EP	— 12.5 $\leq$ Ti $\leq$ 26 7.5 < wt.% Ti < 15	Al + Al <sub>3</sub> Ti	SEM, TEM, Mech SEM, TEM, Mech	35 36
Al-Zr	SM	—	St	Ar	—	EP	— 17.5 $\leq$ Al $\leq$ 40 Al < 15	Am Cryst ESS (Zr)	XRD, DSC, TEM	37
As-Ga	P	5St(15)	St	Ar	—	IC	— BMC AsGa	Am + N-cryst	XRD, DSC, SEM, TEM	38
Au-La B-Co	V P	1St(60) —	WC St	Ar Ar	0.5 g —	ICM EP	— Au <sub>55</sub> L <sub>245</sub> Co <sub>67</sub> B <sub>33</sub>	Am (130 h) Low $E_{\nu}$ Am + cryst High $E_{\nu}$ Am $\rightarrow$ t - Co <sub>2</sub> B	XRD, DSC, TEM	9, 10, 39 40
BCoFeSi	SBM	—	St	He	—	ICM	— B <sub>10</sub> Co <sub>90</sub> <sub>3</sub> Fe <sub>4.7</sub> Si <sub>15</sub>	Am (90 h)	XRD, DSC, TEM	41
BCoFeSi	—	—	—	—	—	—	— B=50, 66.6 BF <sub>2</sub> <sub>2</sub> BF <sub>2</sub> <sub>2</sub>	Am(B) + XCr (60 h) Cryst N-cryst	XRD, SEM, TEM, Mössb	41
B-Cr B-Fe B-Fe	P V SBM	— St(10) —	— St —	Ar Ar —	4 IC EP	— B=20, 34 B=50, 60	— Fe <sub>80</sub> B <sub>20</sub>	Am (30-60 min)	XRD, SEM, TEM, Mössb	42 43 44
B-Fe	V	—	—	—	—	Am	— B <sub>8</sub> Fe <sub>77</sub> Nd <sub>15</sub> Fe + Ni + FeP27.7 + FeB17.8	Cryst (30 h) Am B <sub>8</sub> Fe <sub>40</sub> Ni <sub>40</sub> P <sub>14</sub>	XRD, DSC, Magn XRD, DSC, SEM	46 47
BFeNd	P	St	—	Ar	9.56	EP	— Fe + Ni + FeSi76.2	Am B <sub>12</sub> Fe <sub>39</sub> Ni <sub>39</sub> Si <sub>10</sub>	XRD, DSC, SEM	47
BFeNiP	P	St	St	Ar	9.56	— Fe <sub>78</sub> B <sub>12</sub> Si <sub>9</sub> Fe + Ni + FeB17.8	Cryst (30 h) Fe <sub>3</sub> B + $\alpha$ - Fe	XRD, DSC, SEM XRD, SEM, TEM	48 42	
BFeNiSi	P	St	St	Ar	4	Am EP	— B=50, 66.6 B=66.6	Fe <sub>3</sub> B + $\alpha$ - Fe B <sub>66</sub> Ti <sub>34</sub> Cryst TiB <sub>2</sub>	XRD, DSC, SEM XRD, SEM	49
BFeSi B-Nb	C P	— SBM	St	— St	4 He	EP	— B <sub>65</sub> Cu <sub>70</sub> Y <sub>5</sub> BiFeO <sub>3</sub> + ZnFe <sub>2</sub> O <sub>4</sub>	Am + cryst (10 h) Am + Cryst (250 h) Cryst BiMn (8 h)	XRD, Magn XRD, DSC, SEM SEM, Hardness	44 50 51
B-Ti	SBM	—	—	He	8	EP	— Bi <sub>50</sub> Mn <sub>50</sub>	Cryst TiB	44	
BaCuY	SM	2St(13)	St	Cer	8	EP	— Cu-5vol.%C (graphite)	Am + cryst (10 h) Am + Cryst (250 h) Cryst BiMn (8 h)	XRD, Magn XRD, DSC, SEM SEM, Hardness	52 53
BiFeZnO	P	Cer	Ar	—	5	ORM	— Fe=50, 75, 80	Carbides	Mössb	54
Bi-Mn	SM	St(8)	St	Ar	60-73	EP	— BMC	C=50 C=33	N-cryst Am + N-cryst	44
C-Cu	V	1St(13)	—	—	40	EP	— BMC	—		
C-Fe	SM	(4.8, 1.2)	WC	Ar**	5-10	EP	— BMC	—		
C-V	P	WC	WC	Ar**	40	EP	— BMC	—		
	SBM	—	—	—	—	EP	— BMC	—		

(continued)

TABLE 1. (continued)

A-B	T1	T2	T3	T4	T5	T6	T7	T8	T9	T10	References	
C-W	SBM					EP	—	C=30 C=50 CdTe	N-cryst Am+N-cryst Cryst	XRD, DSC, SEM, TEM	44	
Cd-Te	P	5Sr(15)	St	Ar	—	IC	—	60<Co Co<40	ESS Co(40% Cr) ESS Cr(40% Co)	XRD	38	
Co-Cr	P	—	—	Ar	—	EP	—	Co <sub>50</sub> Gd <sub>50</sub>	Am+cryst	XRD	55	
Co-Gd	P	1WC	WC	Ar	—	IC	Δt	Co <sub>3</sub> Gd	Am+cryst	XRD	56	
Co-Gd	—	—	—	Ar	—	EP	—	Co <sub>7</sub> Gd <sub>2</sub>	Am+cryst	Magn	57	
Co-La	V	Sr(60)	WC	Ar	—	ICM	Δt	Co <sub>62</sub> La <sub>38</sub>	Co+β-La	XRD	9, 10	
Co-Mn	P	—	—	Ar	—	EP	—	ESS Mn(50%Co)	ESS Co(40% Mn)	XRD, DSC, Magn	45	
Co-Nb	A	St	St	—	—	EP	—	Co<85	Am (>40 h)	XRD, DSC, Magn	58	
Co-Nb	P	Sr(12)	St	Ar	10	EP	Δt	Co>85	Cryst (>40 h)	XRD, DSC	59	
Co-Nb	P	—	—	Ar	—	EP	—	20<Co<85	Am 30<Co<85 (30 h)	XRD, DSC, DTA	60	
CoNbZr	A	St	St	Ar	—	EP	—	10<Co<95	Am 35<Co<85 (100 h)	XRD, DSC	61, 62	
CoNbZr	P	—	—	Ar	—	ICM	Δt	Co <sub>87</sub> Nb <sub>5</sub> Zr <sub>5</sub>	Co <sub>81.5</sub> Nb <sub>13.5</sub> Zr <sub>5</sub>	XRD, DSC	63	
CoNbZr	A	S	St	Ar	—	—	—	5<x<13	Am	XRD, DSC	63	
CoNbZr +Y <sub>2</sub> O <sub>3</sub>	A	St	St	Ar	—	—	—	13<x<25	Am+cryst	XRD, Magn	62	
CoNbZr	A	St	St	Ar	—	EP	—	Co <sub>81.5</sub> Nb <sub>13.5</sub> Zr <sub>5</sub> +Y <sub>2</sub> O <sub>3</sub>	Am+cryst Y <sub>2</sub> O <sub>3</sub>	XRD, Magn	62	
CoNiZr +Y <sub>2</sub> O <sub>3</sub>	A	St	St	Ar	—	EP	—	(Co <sub>90</sub> Ni <sub>10</sub> ) <sub>90</sub> Zr <sub>10</sub>	Am (Co <sub>90</sub> Ni <sub>10</sub> ) <sub>90</sub> Zr <sub>10</sub>	XRD, Magn	62	
CoNiZr Co-Sn	SM	St	St	Ar*	5.6	EP	—	(Co <sub>90</sub> Ni <sub>10</sub> ) <sub>75</sub> Zr <sub>25</sub>	Am (Co <sub>90</sub> Ni <sub>10</sub> ) <sub>75</sub> Zr <sub>25</sub>	XRD, Magn	62	
Co-Ti	G	St	St	N <sub>2</sub>	—	EP	Δt	Co <sub>40</sub> Sn <sub>60</sub>	Am+cryst Y <sub>2</sub> O <sub>3</sub>	XRD, Magn	62	
Co-Ti	P	—	St	Ar	13	EP	—	Co <sub>50</sub> Ti <sub>50</sub>	Am (-70 °C, 12 h)	XRD, Ultrason	64	
Co-Ti	A	St	St	—	—	EP	Δt	Co<80	Cryst (RT, 14 h)	XRD	65	
Co-Ti	SM	St	St	Ar	10	ICM	—	Co <sub>50</sub> Ti <sub>50</sub>	Am (64 h)	XRD	66	
Co-V	P	—	—	Ar	—	EP	—	Co <sub>50</sub> Ti <sub>40</sub>	Am (30 h)	XRD, DSC	58	
Co-Y	P	25Sr(14-19)	St	Ar	—	IC	Δt	Co>80	Am (>40 h)	Cryst	67	
Co-Y	P	WC	WC	—	—	IC	—	CoTi+Co <sub>2</sub> Ti	Am Co <sub>60</sub> Ti <sub>40</sub>	XRD, DSC	55	
Co-Zr	P	—	—	—	—	EP	—	Co<40	ESS V(40%Co)	XRD	55	
Co-Zr	P	—	—	Ar	—	EP	—	40<Co<67	Am	EXAFS, Magn	51	
Co-Zr	A	—	—	Ar	—	EP	—	67<Co	ESS Co (33 V)	XRD, Mössb	1	
Co-Zr	P	—	—	—	—	EP	—	YCo <sub>3</sub> , Y <sub>2</sub> Co <sub>7</sub>	Am+cryst (30 h)	XRD	55	
Co-Zr	A	—	—	—	—	EP	—	YCo <sub>5</sub> , Y <sub>2</sub> Co <sub>17</sub>	Am+ESS Zr(4% Co)	XRD	55	
Co-Zr	P	—	—	St	Ar	13	EP	—	92<Co<92	Am+ESS Co(5% Zr)	XRD, DSC, Magn	68, 69
Co-Zr	A	—	—	—	—	EP	—	Co <sub>5</sub> Zr <sub>45</sub>	Am (20 h)	XRD, DSC	58, 70-72	
Co-Zr	P	—	—	—	—	EP	—	75<Co<90	Am (<40 h)	Cryst	58, 70-72	

Co-Zr	G	-	-	-	-	-	-	-	Co <sub>47</sub> Zr <sub>53</sub>	Am	XRD, DSC	73
Cr-Cu	P	St	Ar	4	EP	-	-	Cu+5vol.%Cr	Cu	Cryst (12 h)	XRD, SEM, TEM, Mech	74
Cr-Cu	V	-	St	Ar**	-	EP	$\Delta t$	Atm	30 $\leq$ Cu < 70	N <sub>2</sub> , Grain refinement and amorphization	XRD, TEM	75
Cr-Nb	P	-	-	Ar	4	EP	$\Delta t$	Cr <sub>6.6</sub> Nb <sub>33.3</sub>	Cr <sub>2</sub> Nb (15 h) $\rightarrow$ Am (60 h)	XRD, SEM, TEM	42	
Cr-Nb	P	-	-	Ar	-	EP	$\Delta t$	25 $\leq$ Cr $\leq$ 80	Am 35 $\leq$ Cr $\leq$ 70 (100 h)	XRD, DSC, DTA	60	
Cr-Si	P	-	-	Ar	4	EP	$\Delta t$	Cr <sub>33</sub> Si <sub>66.6</sub>	Cryst CrSi <sub>2</sub> (60 h)	XRD, SEM, TEM	42	
Cr-Ti	P	-	St	Ar	13	EP	-	Cr <sub>60</sub> Ti <sub>40</sub>	Am + cryst (30 h)	XRD, Magn	66	
Cr-Ti	SM	St	Ar	10	ICM	-	-	Cr <sub>63</sub> Ti <sub>37</sub> =Cr <sub>5</sub> Ti <sub>2</sub> +Cr <sub>13</sub> Ti <sub>7</sub>	Am + cryst	XRD, DSC, TEM, SEM	67	
Cr-Zr	V	1St(60)	WC	Ar	-	M	$\Delta t$	-	F.c.c. Zr + Cr	XRD	10	
Cr-Zr	P	-	St	Ar	13	EP	-	Cr <sub>40</sub> Zr <sub>40</sub>	Am + cryst (30 h)	XRD	69	
Cr-Zr	CR	Cu-Er	EF	-	-	Cu <sub>2</sub> Er <sub>28</sub>	-	Am	N-cryst (24 h)	XRD, DSC	76	
Cu-Er	SM	4St	St	Ar	-	IC	-	Cu <sub>Er</sub>	-	XRD, DSC, TEM	29	
Cu-Hf	-	-	St	Ar	-	4	EP	-	30 $\leq$ Cu $\leq$ 70	XRD, DSC	77	
Cu-Mo	P	St	St	Ar	4	EP	-	Cu + 5vol.%Mo	Cryst (12 h)	XRD, EM, Mech	74	
Cu-Nb	P	St	St	Ar	4	EP	-	Cu + 5vol.%Nb	Cryst (12 h)	XRD, SEM, TEM	74	
Cu-Nb	P	-	-	Ar	-	EP	-	Cu = 5, 50	Cryst (>100 h)	XRD, DSC, DTA	60	
CuNbGe	R	WC(10)	WC	Ar	50	EP	$\Delta t$	Cu <sub>44</sub> Nb <sub>42</sub> Ge <sub>14</sub>	Am (24 h)	XRD, TEM	78	
CuNbSi	R	WC(10)	WC	Ar	50	EP	$\Delta t$	Cu <sub>44</sub> Nb <sub>42</sub> Si <sub>14</sub>	Am (24 h)	XRD, TEM	78	
CuNbSn	R	WC(10)	WC	Ar	50	EP	$\Delta t$	Cu <sub>44</sub> Nb <sub>42</sub> Sn <sub>14</sub>	B.c.c. $\rightarrow$ Am (24 h)	XRD, TEM	78	
CuNiTi	P	3WC(15)	WC	-	10	EP	-	Cu <sub>5</sub> Ni <sub>40-x</sub> Ti <sub>60</sub>	Am x = 20	XRD, TEM	79	
Cu-Ru	SM	St	Ar	-	EP	$\Delta t$	-	x = 10, 30	Am + cryst	XRD, DSC	24	
Cu-Ta*	P	St(11)**	St**	Ar	4	EP	$\Delta t$	Cu <sub>40</sub> Ru <sub>60</sub>	Cubic (92 h)	XRD, DSC	24	
Cu-Ta*	V	CB(10)	CB	Ar	-	EP	$\Delta t$	Cu <sub>70</sub> Ru <sub>30</sub>	Cubic + Ms(?) (130 h)	XRD, DTA, SEM	80	
Cu-Ta*	P	St	St	Ar	4	EP	$\Delta t$	Cu=20, 30, 40, 50	Am + Cu + Ta	XRD, NeutrsEXAFS	43	
Cu-Ta*	P	CB(10)	CB	Ar	-	EP	$\Delta t$	Cu <sub>30</sub> Ta <sub>70</sub>	Am ( $\Delta t$ > 100 h)	XRD, SEM, TEM, Mech	74	
Cu-Ta*	SM	-	St	Ar	7	EP	$\Delta t$	Cu <sub>30</sub> Ta <sub>70</sub>	Am (120 h)	XRD, DSC, EXAFS	81	
Cu-Ta*	P	CB(10)	CB	Ar	-	EP	$\Delta t$	Cu <sub>50</sub> Ti <sub>40</sub>	Am (29 h)	XRD, DSC	24,	
Cu-Ti	SM	St	St	Ar	-	EP	$\Delta t$	Cu <sub>37</sub> Ti <sub>13</sub>	F.c.c. Cu(Ti) (28 h)	RX, DSC, Magn	66	
Cu-Ti	P	-	St	Ar	13	EP	-	Cu <sub>50</sub> Ti <sub>40</sub>	Am (30 h)	XRD, DSC, SEM, TEM	67	
Cu-Ti	SM	P	WC(3-10)	St*	Ar	3-10	EP	-	Am Co <sub>60</sub> Ti <sub>40</sub>	Am Co <sub>60</sub> Ti <sub>40</sub>	XRD, SEM, DSC	84
Cu-V*	P	S	St	Ar	4	EP	-	10 $\leq$ Cu $\leq$ 87	Am (9 h)	XRD, SEM, TEM, Mech	74	
Cu-V*	P	20CB(11)	CB	Ar	20 g	EP	$\Delta t$	Cu <sub>50</sub> V <sub>50</sub>	Am (120 h)	XRD, DSC, Neutron DTA	85	
Cu-W*	P	5St(15)	St	Ar	10 g	EP	-	0 $\leq$ Cu $\leq$ 100	Am + cryst	XRD, SEM-TEM, DTA	86	
Cu-W*	P	St	St	Ar	4	EP	-	Cu + 5vol.%W	Cryst (12 h)	XRD, SEM, TEM	74	
Cu-Y	SM	2St(13)	St	He	8	EP	-	(15 $\leq$ Y $\leq$ 67)	10 h	XRD, DSC	50	
Cu-Zn	SM	St(8)	St	Ar	5	EP	-	Y = 28	Am	Cryst (CuY + Y)	87	
Cu-Zn								Cu = 50, 52.5 <sup>w</sup>		B <sub>2</sub> CuZn + Martensite (3 h)		

(continued)

TABLE 1. (continued)

A-B	T1	T2	T3	T4	T5	T6	T7	T8	T9	T10	References
Cu-Zn	P	CB	CB	Ar	-	IC	Δt	Cu <sub>5</sub> Zn <sub>8</sub>	Cryst (60 h)	XRD, DSC	88
Cu-Zn	WC	WC	WC	Ar	-	EF	-	18 < Cu ≤ 75	Cryst	XRD, TEM	89
Cu-Zr	WC	WC	St	Ar	13	EP	-	Cu <sub>60</sub> Zr <sub>40</sub>	Am (20 h)	XRD, DSC	90
Cu-Zr	P	20St*(8)	St*	Ar	10	EP	-	Cu <sub>60</sub> Zr <sub>40</sub>	Am (13 h)	XRD, DSC	68, 91
Cu-Zr	SM	St	St	Ar	10	ICM	-	Cu=40, 50, 60	Am (13–15 h)	Magn	68, 91
Cu-Zr	SM	St	St	Ar	10	ICM	-	CuZr, Cu <sub>3</sub> Zr <sub>2</sub>	Am Cu <sub>40</sub> Zr <sub>60</sub>	XRD, DSC, SEM, TEM	67
Cu-O–Fe	SM	3St(8g)	St	Ar	3	-	-	+ Cu <sub>5</sub> <sub>1</sub> Zr <sub>1.4</sub>	Fe <sub>3</sub> O <sub>4</sub> + Cu	SEM-EDX	15
Cu-O–Ti	SM	3St(8g)	St	Ar	3	-	-	CuO + Ti	TiO <sub>2</sub> + Cu	SEM-EDX	15
Fe-Nb	-	-	Ar	-	EP	-	-	5 ≤ Fe ≤ 85	Am 35 ≤ Fe ≤ 75 (100 h)	XRD, DSC, DTA	60
Fe-Si	P	St(9.5)	St	Ar	12	EP	Δt	Fe <sub>75</sub> Si <sub>25</sub>	Am (?)	XRD, DSC, SEM, Magn	92
Fe-Sm–V	P	St	Ar	EP	-	Fe <sub>70</sub> Sm <sub>15</sub> V <sub>15</sub>	Cryst (64 h)	XRD, Magn	93		
Fe-Ti	G	St	N <sub>2</sub>	-	EP	Δt	Fe <sub>50</sub> Ti <sub>50</sub>	Am (64 h)	XRD, DSC, SEM	65	
Fe-Ti	P	-	St	Ar	13	EP	-	Fe <sub>60</sub> Ti <sub>40</sub>	Am + cryst (30 h)	XRD, Magn	66
Fe-Ti	SM	St	St	Ar	10	ICM	-	FeTi + Fe <sub>2</sub> Ti	Am Fe <sub>60</sub> Ti <sub>40</sub>	XRD, DSC, SEM, TEM	67
Fe-V	SM	WC	WC	N <sub>2</sub>	6	EP	Δt	Fe <sub>50</sub> V <sub>50</sub>	Am + cryst (50 h)	XRD, TEM, Mössb	94
Fe-V	SM	WC	WC	Ar**	5–10	EP	-	Fe <sub>50</sub> V <sub>50</sub>	Am + N-cryst (48 h)	Mössb	54
Fe-Zr	P	St(10)	St	Ar	10	EP	Δt	Fe <sub>66</sub> Zr <sub>33</sub>	Am	XRD	95
Fe-Zr	P	-	-	-	IC	-	FeZr <sub>2</sub>	Am + cryst (60 h)	XRD	96	
Fe-Zr	P	St(10)	St	Ar	13	EP	Δt	20 < Fe ≤ 80	Am (60 h)	XRD, DSC, Magn	68, 69, 97
Fe-Zr	P	-	St	Ar	13	EP	-	30 ≤ Fe ≤ 78	Am	XRD, Mössb	98
Ge	P	5St(15)	St	Ar	10 g	EP	Δt	80 ≤ Fe ≤ 95	Am + cryst	XRD, SEM, TEM	99
Ge–Nb	SM	-	-	-	EP	Δt	Ge <sub>25</sub> Nb <sub>75</sub>	cryst Ge	XRD, TEM	100	
Ge–Nb	-	-	-	-	EP	Δt	Am + cryst (13 h)	Am + cryst	XRD, TEM	101	
Ge–Pb*	SM	St(8)	St	Ar	6	EP	Δt	0 ≤ Ge ≤ Pb	Am (?) + cryst (32 h)	XRD, DSC, TEM	102
Ge–Si	SM	St*(8)	St*	Ar*	5	EP	Δt	0 ≤ Ge ≤ 100	Cryst Ge <sub>100-x</sub> Si <sub>x</sub> (8 h)	XRD, DSC, SEM	52, 103
Ge–Si	P	5St(15)	St	Ar	10 g	EP	-	Ge = 25, 50, 75 <sup>w</sup>	Am + N-cryst	XRD, DSC, DTA, EM	104
Ge–Sn*	SM	St(8)	St	Ar	6	EP	Δt	0 ≤ Ge ≤ 100	Am + cryst (32 h)	XRD, DSC, TEM	102
Ge–Sn*	SM	St(8)	St	Ar	6	EP	Δt	Sn = 10, 50, 70	Cryst (60 h)	XRD, DSC, SEM, TEM	105
La–Ni	V	1St(60)	WC	Ar	-	M	Δt	La = 34, 43	β-La + Ni	XRD	9, 10
Mg–Ni	WC	WC	St	Ar	-	EF	-	0.5 ≤ Mg < 0.8	Am Mg <sub>60</sub> Ni <sub>40</sub>	XRD, DSC, SEM	106
Mg–Ti	SM, A	St	St	Ar	-	EP	Δt	TiMg <sub>9</sub> W <sub>t</sub>	Ms f.c.c. Ti(6% Mg)	XRD, DSC, DTA, TEM	107
Mg–Zn	SBM	-	-	He	ICM	Δt	MG <sub>70</sub> Zn <sub>30</sub>	Am (58 h)	XRD, RBS, DSC, SEM	108	
Mn–Nb	P	-	-	Ar	-	EP	-	45 ≤ Mn < 55	Am (100 h)	XRD, DSC, DTA	60
Mn–Si	SM	St	St	Ar	10	ICM	-	Mn <sub>54</sub> Si <sub>46</sub> = MnSi + Mn <sub>3</sub> Si <sub>3</sub>	Cryst	XRD	67

Mn-Ti	P	-	St	Ar	13	EP	-	Mn <sub>60</sub> Ti <sub>40</sub>	Am + cryst α-Fe (30 h)	XRD, Magn	66, 68
Mn-Ti	SM	St	St	Ar	10	ICM	-	Mn <sub>2</sub> Ti <sub>1</sub> + Mn <sub>5.2</sub> Ti <sub>4.8</sub>	Am Mn <sub>62</sub> Ti <sub>38</sub>	XRD, DSC, SEM, TEM	67
Mn-Zr	P	St	St	Ar	13	EP	-	Mn <sub>60</sub> Zr <sub>40</sub>	Am (30 h)	XRD, DSC	69
Mo-Ni	SM	St	St	Ar	10	EP	Δt	Mo <sub>50</sub> Ni <sub>50</sub>	Am + cryst (28 h)	XRD, EXAFS	24, 109
Mo-Ni	SM	WC	Ar	-	EP	Δt	Mo <sub>15</sub> Ni <sub>85</sub>	ESS Ni(13% Mo) (20 h)	XRD, SEM	110	
Nb-Ni	WC	St(9.5)	St	Air	-	EF	Δt	Mo <sub>40</sub> Ni <sub>60</sub>	ESS Ni(23% Mo) (40 h)	XRD	111
Nb-Ni	SM	St(8)	St	Ar*	3–10 g	EP	-	Nb <sub>40</sub> Ni <sub>60</sub>	Am + Ni + Nb + Ni <sub>3</sub> Nb	DSC	2
Nb-Ni	SM	St(8)	St	Ar*	10	EP	-	Nb <sub>40</sub> Ni <sub>60</sub>	Am (14 h)	XRD, DSC, TEM	112
Nb-Ni	P	St(15–20)	St	Ar	30 g	EP	Δt	Nb <sub>40</sub> Ni <sub>60</sub>	Am + cryst	XRD, EXAFS	113
Nb-Ni	P	St	St	Ar	4	EP	Δt	Nb <sub>40</sub> Ni <sub>60</sub>	Am 0.2 < Ni < 0.9	XRD, DSC, SEM, TEM	114, 115
Nb-Ni	P	-	-	Ar	-	EP	-	Nb <sub>33.3</sub> Si <sub>66.6</sub>	Am 20 < Nb < 90	XRD, DSC, DTA	60
Nb-Si	P	-	-	Ar	-	EP	Δt	Nb <sub>75</sub> Sn <sub>25</sub>	NbSi <sub>2</sub> → Am	XRD, SEM, TEM	42
Nb-Sn	SM	St*(8)	St*	Ar*	4, 6, 8	EP	Δt	Nb <sub>75</sub> Sn <sub>25</sub>	Nb <sub>3</sub> Sn → Am (100 h)	XRD	101
Nb-Sn	R	WC(10)	WC	Ar	50	EP	Δt	Ni <sub>3</sub> Er <sub>27</sub>	Am (24 h)	XRD, DSC	78
Ni-Er	CR	-	-	-	-	EF	-	15 < Ni < 65	Am (18 h)	XRD, DSC	76
Ni-Hf	SBM	-	-	WC	Ar	EP	Δt	Ni <sub>50</sub> Si <sub>50</sub>	Ni + Si	XRD, DSC, EDX	77
Ni-Si	V	1S(60)	WC	Ar	IC	IC + EP	-	Ni <sub>3</sub> Sn	Am (114 h)	EDX	44
Ni-Sn	SM	-	-	-	-	EP	-	Ni <sub>3</sub> Sn + Ni <sub>3</sub> Sn + Sn	Am + Ni(Sn) (144 h)	XRD, DSC, EDX	116
Ni-Sn	SM	-	-	-	-	EP	-	Ni <sub>3</sub> Sn + Sn	Am + Ni <sub>3</sub> Sn <sub>2</sub>	XRD, SEM, TEM	117
Ni-Ti	SM	-	St	Ar	-	EP	Δt	60 < Ni < 80	Am + μ-cryst	XRD, SEM, TEM	117
Ni-Ti	SM	60St(6)	St	Ar	10 g	EP	Δt	Ni <sub>75</sub> Sn <sub>25</sub>	Am (12–17 h)	XRD, DSC	118, 119
Ni-Ti	SM	-	St	Ar	-	EP	Δt	Ni = 35, 45, 50	Am (> 11 h)	XRD, Neutron	120
Ni-Ti	G	St	St	N <sub>2</sub>	-	EP	Δt	Ni <sub>50</sub> Ti <sub>50</sub>	35 < Ni < 60	XRD	33
Ni-Ti	SM	-	St	Ar	-	EP	Δt	Ni <sub>50</sub> Ti <sub>50</sub>	Am (16 h)	XRD, DSC, SEM	65
Ni-Ti	P	-	St	Ar	13	EP	Δt	Ni <sub>50</sub> Ti <sub>50</sub>	Ni <sub>75</sub> Sn <sub>25</sub>	XRD, EXAFS	121, 122
Ni-Ti	SM	4St	St	Ar	-	IC	-	Ni <sub>60</sub> Ti <sub>40</sub>	Am (30 h)	XRD, DSC, Magn	66
Ni-Ti	A	-	St	Ar	-	IC	E, ν	Ni <sub>11</sub> Ti	Ni <sub>3</sub> Sn	XRD, DSC, TEM	29
Ni-Ti	CR	-	St	Ar	-	IC	-	Ni <sub>50.8</sub> Ti <sub>49.2</sub>	Am + N-cryst	TEM, HRTEM	61
Ni-Ti	SM	St	Ar	10	ICM	-	-	NiTi + N <sub>3</sub> Ti	Am Ni <sub>60</sub> Ti <sub>40</sub>	XRD, DSC, SEM, TEM	123
Ni-Ti	SM	60St(6)	St	Ar	10 g	EP	Δt	Ni <sub>33</sub> Ti <sub>67</sub>	Am	XRD, DSC, SEM	124–126
Ni-Ti	CR	20St(14)	St	Ar	30 g	EP	Δt	NiT <sub>2</sub>	Am	DSC, TEM	127
Ni-V	P	1S(60)	WC	Ar	EP	Δt	Ni <sub>50</sub> Ti <sub>50</sub>	Am (800 h)	XRD, DSC, Neutron	128	
Ni-Zr	WC	V	1S(60)	WC	EP	E <sub>ν</sub>	-	Ni <sub>62</sub> Zr <sub>38</sub>	Ni = 62, 68	XRD, DSC	90
Ni-Zr	SM	-	-	-	EP	Δt	Ni <sub>62</sub> Zr <sub>38</sub>	Am (70 h)	XRD, DSC, SEM-EDX	10	
								Ni <sub>10</sub> Zr <sub>7</sub> + Ni <sub>21</sub> Zr <sub>8</sub>	Am Ni <sub>61</sub> Zr <sub>39</sub> (21 h)	(continued)	

TABLE 1. (continued)

A-B	T1	T2	T3	T4	T5	T6	T7	T8	T9	T10	References
Ni-Zr	WC										
Ni-Zr	–	St	St	Ar	4	EP	–	Ni=61 Ni=64 Ni=71 20≤Ni≤70	Am+cryst (?) Am Am+cryst (?) + Ni Am	XRD, DSC, TEM	111, 129
Ni-Zr	V	St*(63)	St	V <sub>ac</sub> Ar*	5 g 5 g	IC ICM	–	Ni=80 Ni <sub>10</sub> Zr <sub>7</sub> NiZr <sub>2</sub>	Am+cryst (?) Am AM Ni <sub>50</sub> Zr <sub>50</sub> AM Ni <sub>40</sub> Zr <sub>60</sub>	XRD, SEM XRD, SEM, DSC	130 131 52
Ni-Zr	SM	St	St	Ar	15	EP	Δt	0≤Ni<100 0<Ni≤100	Am 20–30<Ni<75–85 Am, or am+cryst	XRD, DSC XRD, DSC, SEM, TEM	132 133
Ni-Zr	P	St	St	Ar	10 g	EP	Δt	0<Ni≤100	Am, or am+cryst	XRD, DSC, SEM, TEM	134
Ni-Zr	P	5St(15)	St	Ar	10 g	IC	Δt	0<Ni≤100	Am, or am+cryst	XRD, DSC, SEM, TEM	134
Ni-Zr	SBM	5St(15)	St	Ar	10 g	ICM	E, ν Δt, E, ν, T	Ni <sub>10</sub> Zr <sub>7</sub> , Ni <sub>11</sub> Zr <sub>9</sub>	Am F <sup>ct</sup> (E, ν, T) Am (60 h)	XRD	135
Ni-Zr	P	–	St	Ar	–	EP	–	35≤Ni≤83 27≤Ni≤78	Am (20 h)	XRD, H <sub>2</sub> probe	136
Ni-Zr	P	–	St	Ar	13	EP	–	Ni <sub>33.3</sub> Zr <sub>66.6</sub>	Am (10 h)	XRD, DTA	68, 69
Ni-Zr	SM	3St	St	Ar	7 g	EP	–	Ni <sub>61</sub> Zr <sub>39</sub>	Am (16 h)	XRD	137
Ni-Zr	A	St	St	Ar	–	EP	–	24≤Ni≤85	Am	XRD	62
Ni-Zr	SM	St	St	Ar	10	EP	–	10≤Ni≤22	Am+Zr (Ni)	XRD, DSC	67, 138, 139
Ni-Zr	V	S(10)	St	Ar	20 g	EP	T	Ni <sub>11</sub> Zr <sub>9</sub> +NiZr <sub>2</sub>	Am Ni <sub>40</sub> Zr <sub>60</sub> (8 h) Am Ni <sub>50</sub> Zr <sub>50</sub> (18 h)	XRD, DSC	43, 87, 140
Ni-Zr	P	5St(15)	St	Ar	10 g	EP, ICM	Δt	Ni <sub>50</sub> Zr <sub>50</sub> NiZr <sub>2</sub>	Am+cryst –120 °C≤T≤200 °C	XRD, DSC XRD, DSC, SEM, TEM	141 142–144
Ni-Zr	P	St	St	Ar	4	EP	Δt	40<Ni<60	Am (60 h)	Am (120 h)	
Ni-Zr	V	St(60)	St	Ar	15	ICM	–	30<Ni<70 Reversibility (?)	Am → Am+cryst Am (Ni <sub>78</sub> Zr <sub>22</sub> ) → am+cryst	XRD, DSC, Auger XRD, EXAFS XRD, DSC, EPMA, Magn	145, 146 51 147–149
Ni-Zr	SM	St	St	Ar	7 g	EP	Δt	Ni <sub>61</sub> Zr <sub>39</sub> Ni <sub>5</sub> Zr <sub>2</sub> +Ni <sub>7</sub> Zr <sub>2</sub>	Am (8 h)	XRD, DSC, Auger	145, 146
Ni-Zr	–	25St	St	Ar	–	EP, IC	Δt	Ni <sub>50</sub> , Ni <sub>7</sub> Zr 34<Ni<78	Am Ni <sub>50</sub> Zr <sub>50</sub> (400 h)	XRD, EXAFS	51
Ni-Zr	P	12St(10)	St	Ar	–	ICM	Δt	Ni <sub>50</sub> Zr <sub>50</sub>	Am+cryst Am (20 h)	XRD, DSC, EPMA, Magn	147–149
Ni-Zr	V	St(60)	St	Ar	–	0.5 g	ICM	–	Ni <sub>10</sub> Zr <sub>7</sub> +Ni <sub>21</sub> Zr <sub>8</sub>	XRD, DSC	149, 150
Ni-Zr	V	St	St	Ar	1–2 g	EP	BMC	Ni <sub>52</sub> Zr <sub>38</sub>	Am	XRD, DSC	151
Ni-Zr	CR	St	St	Ar	–	EF	–	Ni <sub>22</sub> Zr <sub>78</sub>	Am+cryst (?)	XRD, DSC, TEM	127
Ni-Zr	A	St	St	Ar	–	Am	–	Am Ni <sub>61</sub> Zr <sub>39</sub> +Y <sub>2</sub> O <sub>3</sub>	Am+cryst Y <sub>2</sub> O <sub>3</sub> (21 h)	XRD	61, 62
Pd-Si	P	St(10)	St	Ar	10	EP	–	Pd <sub>80</sub> Si <sub>20</sub>	Am+cryst	XRD, SEM-EDX	152

Pd-Ti	V	WC	WC	Ar	5	ICM	$\Delta t$	42 $\leq$ Ti $\leq$ 85 Ti = 35 45 $\leq$ Pd 45 $>$ Pd Pt <sub>50</sub> Sb <sub>50</sub>	Am (17 h) Am + cryst Am (60 h) Am + PdZr <sub>2</sub> Am + cryst Cryst (32 h) Ni-cryst (24 h) Am + N-cryst (70 h)	XRD, DTA	153
Pd-Zr	V	—	—	—	—	ICM	—	—	—	XRD, EDX	154
Pt-Sb	WC	St	St	Ar	—	EF	—	—	XRD, DSC, SEM	111	
Ru	SM	St	St	Ar	13	IC	$\Delta t$	RuSi (CsCl)	XRD, TEM, DSC	30	
Ru-Si	SM	4St	St	Ar	10 g	—	—	—	XRD, TEM, DSC	97	
Si	P	St	St	Ar	10 g	—	—	SEM-TEM	XRD, DSC, SEM-TEM	155	
Si-Ti	P	St	St	Ar	10	EP	$\Delta t$	Si <sub>37</sub> Ti <sub>62.5</sub> Si <sub>67</sub> Ti <sub>33</sub>	N-cryst Si <sub>3</sub> Ti <sub>3</sub> (200 h) Ms N-cryst b.c.c.	XRD	23
Si-Ti	SBM	—	—	Ar	—	EP	$\Delta t$	—	—	XRD	44
Si-Ti	P	St	St	Ar	15	EP	$\Delta t$	20 $\leq$ Si $\leq$ 80 70 $\leq$ Si $\leq$ 100	Am 25 $<$ Si $<$ 60 (25 h) Am + Si(Sn) + Sn(Si)	XRD, DSC, SEM	156
Si-Sn*	P	5S(15)St	—	Ar	10 g	EP	—	—	—	XRD, DSC, SEM, TEM	157
Si-Zn*	P	5St(15)	St	Ar	10 g	EP	—	70 $\leq$ Si $<$ 100	Am + Si(Zn) + Zn(Si)	XRD, DSC, SEM, TEM	157
Si-Zr	—	—	—	St	—	—	—	—	Cryst (163 h) ESS cryst (30 h)	XRD	73
Ti-V	P	—	—	St	Ar	13	EP	—	Cryst (30 h)	XRD	66
V-Zr	P	St	St	Ar	13	EP	—	—	—	XRD, DTA	69
V-Zr	V	—	—	—	—	EP	—	—	Am + cryst Am (140 h)	XRD, DSC	73, 148

rolling) are still not well understood. Nevertheless, from a practical point of view, these mechanical methods allow the production of new amorphous phases or crystalline phases with extended composition domains. The processes are used for the production of bulk materials such as composite materials which are reinforced by intermetallic compounds at the nanometer scale (for a recent review see ref. 162).

Based on analysis of X-ray diffraction (XRD) patterns, we report on the solid-state phase transition induced by mechanical alloying and/or post milling annealing in an Fe–Si powder mixture. The first part of the work deals with the influence of composition on the structure of the as MA end-product. By analogy with amorphization induced by solid-state diffusion occurring during annealing of multilayer systems, the second part deals with the structure of the end-product produced by annealing MA powders for a short duration and with the influence of the grain size and residual strain of the as-milled iron and silicon crystalline phases on the structure of isothermally annealed MA powders. Specific attention was paid to two particular phases exhibiting interesting physical properties: Fe(Si) (a crystalline phase exhibiting a magnetic effect) and  $\beta$ -FeSi<sub>2</sub> (a semiconductor-type phase exhibiting a direct optical gap and thermoelectric power) crystalline phases.

## 2. Experimental details

### 2.1. Milling conditions corresponding to determination of the influence of composition on the stationary end-product structure

The MA processes corresponding to determination of the influence of composition on the stationary end-product structure were carried out using a classical Fritsch planetary high energy ball-milling machine (Pulverisette P5/2). The chosen intensity setting will be referred to later as P5/2(10).  $\Omega$  (rev min<sup>-1</sup>) is the rotation speed of the disc on which the vial holders were fixed. The vial holders turned at a rotation speed  $\omega$ . The  $\Omega$  rotation radius was equal to  $R_\Omega$ . Therefore the shock kinetic energy was proportional to  $\Omega^2 R_\Omega$ . The value of  $\Omega$  was checked by a tachometer. The specific parameters are given in Table 2.

10 g of a mixture of pure iron powder (Prolabo, R.P. Normapur) and of pure silicon (hyperpure polycrystalline silicon, Wacker Chemitronic, GmbH, 300  $\Omega$  cm n-type and 3000  $\Omega$  cm p-type) pieces with the compositions listed in Table 3, were introduced into a cylindrical tempered steel container of capacity 45 ml. This procedure was performed in a glove box filled with purified argon. Each container was loaded with five balls (diameter 1.5 cm, mass 14 g). The containers were sealed in the glove box with a Teflon O-ring and

TABLE 2. Mechanical alloying parameters corresponding to the various milling conditions

MA conditions	$\Omega$ (rev min <sup>-1</sup> )	$R_\Omega$ ( $\times 10^{-2}$ m)	$\omega$ (rev min <sup>-1</sup> )	$\Omega^2 R_\Omega$ (m s <sup>-2</sup> )
P5/2(10)	340	12	765	153.8
G7( $\Omega/\omega/\Delta t$ ) <sup>a</sup>	700	6.75	250	362.4
	600	6.75	250	266.2
	500	6.75	250	184.9

<sup>a</sup> $\Delta t$  corresponding to the MA duration is noted in the end product table.

the milling thus proceeded in a stationary argon atmosphere. In order to study the influence of the initial state on the end-product (*i.e.* a mixture of elemental component powders or a pre-alloyed powder), some experiments were performed starting from melt spun ribbons. Table 4 lists the initial compositions and the related phase structure corresponding to the as-melt-spun ribbons.

### 2.2. Post-milling annealing induced end product study

By analogy with the solid-state phase transition occurring during the annealing of a multilayer Fe/Si system [163–170], the purpose of this study was to analyse the effect of isothermal annealing on a mixture of iron and silicon crystalline phases which had been obtained by a short duration milling process. Furthermore, the influence of the residual strains and the ranges of grain size of the as-milled iron and silicon crystalline phase on the end-product annealing structure was investigated. In order to obtain such specific powder mixtures, a special high energy planetary machine (hereafter referred to as the G7 machine) was used. Indeed, the frequency and energy of the shocks occurring during the process may be selected independently. This machine was previously used to determine the parameter phase diagram of the ball-milled Ni<sub>10</sub>Zr<sub>7</sub> phase [135]. In the present work, the energy (*i.e.* the value of  $\Omega$ ) was the experimented parameter (see Table 2).

Durations of the mechanical process were chosen to avoid the formation of a large silicide phase, *i.e.* the end-product MA structure should be a mixture of iron and silicon crystalline phases. Thus, short MA duration processes (1 up to 6 h), depending on the selected energy and frequency conditions were performed (see Table 6).

The post-milling annealing procedure was carried out in vacuum ( $8 \times 10^{-8}$  Torr) for 24 h and the isothermal annealing temperatures were 300 °C, 500 °C and 800 °C.

TABLE 3. End product characterization as a function of the initial composition, starting from a mixture of the elemental powders corresponding to the P5/2(10) milling condition and a process duration of 168 h; determination of the end-product composition, the container contamination (expressed in chromium content) and the end product phase mixture (crystalline and amorphous phases)

Initial Si content	End-product Si content (wt.%)	Cr content (wt.%)	End-product structure	
			Crystalline phases (related lattice parameter in nm)	Amorphous phases (at.%) (first halo position in nm)
5	6.6 ± 0.5	<0.5	α-Fe(Si) ( $a = 0.2863 \pm 0.0001$ )	Fe <sub>95</sub> Si <sub>5</sub> ( $d = 0.1997$ (wt.%))
10	10.0 ± 0.3	<0.3	α-Fe(Si) ( $a = 0.2853 \pm 0.0001$ )	Fe <sub>90</sub> Si <sub>10</sub> ( $d = 0.2012$ ) (wt.%)
15	16.1 ± 0.5	<0.2	α-Fe(Si) ( $a = 0.2846 \pm 0.0002$ )	Fe <sub>85</sub> Si <sub>15</sub> ( $d = 0.2007$ ) (wt.%)
16	16.1 ± 0.5	<0.1	α-Fe(Si) ( $a = 0.2837 \pm 0.0002$ )	Fe <sub>84</sub> Si <sub>16</sub> ( $d = 0.2011$ ) (wt.%)
17	17.6 ± 0.5	<0.3	Fe <sub>3</sub> Si ( $a = 0.5655 \pm 0.0001$ )	Fe <sub>75</sub> Si <sub>25</sub> ( $d = 0.2000$ )
18	17.9 ± 0.1	<0.3	Fe <sub>3</sub> Si ( $a = 0.5653 \pm 0.0001$ ), η-Fe <sub>5</sub> Si <sub>3</sub>	Fe <sub>75</sub> Si <sub>25</sub> ( $d = 0.2000$ )
20	21.2 ± 2.5	<0.5	Fe <sub>3</sub> Si ( $a = 0.5647 \pm 0.0001$ )	Fe <sub>75</sub> Si <sub>25</sub> ( $d = 0.2000$ )
30	24.7 ± 1.0	n.d.	FeSi ( $a = 0.454 \pm 0.006$ ) η-Fe <sub>5</sub> Si <sub>3</sub> , Fe <sub>2</sub> Si, Fe <sub>3</sub> Si	Fe <sub>50</sub> Si <sub>50</sub> or Fe <sub>62.5</sub> Si <sub>37.5</sub> ( $d = 0.2005$ )
40	23.6 ± 3.5	<0.7	FeSi, η-Fe <sub>5</sub> Si <sub>3</sub>	Fe <sub>50</sub> Si <sub>50</sub> or Fe <sub>62.5</sub> Si <sub>37.5</sub> ( $d = 0.1994$ )
50	31.6 ± 0.2	n.d.	FeSi ( $0.4493 \pm 0.0001$ ), η-Fe <sub>5</sub> Si <sub>3</sub>	Fe <sub>50</sub> Si <sub>50</sub> or Fe <sub>62.5</sub> Si <sub>37.5</sub> ( $d = 0.1985$ )
60	80.0 ± 2.0	<0.1	α-FeSi <sub>2</sub> , Si, X(?)	α-Fe <sub>33.3</sub> Si <sub>66.6</sub> ( $d = 0.1843$ ), (?) ( $d = 0.4193$ )
70	71.5 ± 1.0	<0.1	α-FeSi <sub>2</sub> , β-FeSi <sub>2</sub> , Si	α-Fe <sub>33.3</sub> Si <sub>66.6</sub> ( $d = 0.1871$ ), Si ( $d = 0.3369$ ) β-Fe <sub>33.3</sub> Si <sub>66.6</sub> ( $d = 0.4938$ )
80	82.2 ± 2.0	<0.2	α-FeSi <sub>2</sub> , Si, X(?)	α-Fe <sub>33.3</sub> Si <sub>66.6</sub> ( $d = 0.1887$ , (?) ( $d = 0.4233$ ))
85	86.4 ± 0.2	n.d.	α-FeSi <sub>2</sub> , Si, X(?)	α-Fe <sub>33.3</sub> Si <sub>66.6</sub> ( $d = 0.1732$ ), (?) ( $d = 0.4178$ )
90	88.6 ± 1.5	<0.2	α-FeSi <sub>2</sub> , FeSi, Si	α-Fe <sub>33.3</sub> Si <sub>66.6</sub> ( $d = 0.1875$ ), (?) ( $d = 0.3907$ )
95	96.8 ± 0.2	<0.1	α-FeSi <sub>2</sub> , Si	α-Fe <sub>33.3</sub> Si <sub>66.6</sub> ( $d = 0.1820$ )

n.d., not detectable.

TABLE 4. End-product structure corresponding to the milled melt-spun ribbons

Initial Si content (wt.%)	End-product Si content (wt.%)	Cr content (wt.%)	Initial structure	End-product phases	
				Crystalline	Amorphous
10	9.5 ± 0.5	<0.5	Fe <sub>3</sub> Si ( $a = 0.564$ )	α-Fe(Si)	Fe(Si)
30	22.9 ± 0.1	<0.8	η-Fe <sub>5</sub> Si <sub>3</sub> , FeSi ( $a = 0.446$ )	Fe <sub>2</sub> Si, FeSi α-FeSi <sub>2</sub>	Fe <sub>50</sub> Si <sub>50</sub>
50	30.6 ± 0.5	<0.9	FeSi ( $a = 0.446$ )	Fe <sub>5</sub> Si <sub>3</sub> , FeSi	Fe <sub>50</sub> Si <sub>50</sub> or Fe <sub>62.5</sub> Si <sub>37.5</sub>
70	68.7 ± 0.5	<0.1	β-FeSi <sub>2</sub> β-FeSi <sub>2</sub> , Si	α-FeSi <sub>2</sub> , Si	–

### 2.3. Chemical microanalyses (EDX/SEM)

In order to evaluate possible container contamination or depletion of elements which may have occurred owing to friction of the particles on the balls and the walls of the container, EDX analyses were performed using an Si-Li detector and a TRACOR EDX analyser in conjunction with a scanning electron microscope (ZEISS DSM 950). A semi-quantitative program with internal references (SQ from TRACOR) was used to analyse the EDX/SEM spectra.

### 2.4. X-ray investigations

After continuous milling, a small amount of the MA powder was extracted from the container and glued onto a silica plate for further X-ray investigations. The XRD patterns were obtained using a ( $\theta$ - $2\theta$ ) Philips diffractometer with Co K $\alpha$  radiation ( $\lambda = 0.17889$  nm).

The acquisition conditions were  $\Delta(2\theta) = 0.1^\circ$ , and  $\Delta t/\text{step}(2\theta) = 40$  s.

The Bragg expression was applied to determine the  $d$  value corresponding to the diffraction peak position  $\theta$ :

$$\lambda = 2d \sin \theta$$

The effective diameter of the particles  $\Phi$  was calculated from the Scherrer expression:

$$\Phi = 0.91\lambda/(B \cos \theta)$$

where  $B$  is the linewidth (expressed in  $2\theta$ ) of the considered crystalline peak.

A numerical method, the ABFFit program (for an explanation of the use and details of the deconvolution based on this program see ref. 155), was used to analyse the XRD patterns and to obtain the position and the

full width at half-height (FWHH) of the various peaks. As shown by Gaffet and Harmelin [155], such a deconvolution does not depend qualitatively on the chosen peak shapes (*i.e.* gaussian, Lorentz or Cauchy). Therefore, the gaussian type peak deconvolution was selected to analyse the XRD patterns. It is obvious that this XRD deconvolution method does not allow the grain size and the strain effects, which are well known to contribute both to the shape and to the width of the diffraction peaks, to be distinguished.

Therefore, in the particular case of the post-milling annealing experiments, another deconvolution method was used to analyse the XRD patterns and to characterize the end-product structure, the automated powder diffraction method (so-called APD method, developed by Philips). This numerical APD method was able to analyse the XRD peak concerned in terms of grain size and strain effects. Nevertheless, this method works as a “blind black box” and particular attention was paid to the interpretation of the deconvolution results. Taking into account the mentioned caution, the results were used to characterize effectively the effect of the milling energy (*i.e.* the value of  $\Omega$ ) on the grain size and the strain contribution of the iron and silicon crystalline phases.

In particular cases, the presence of an amorphous phase was detected as a component of the end-product mixture. This was detected using both deconvolution methods.

### 3. Results and discussion

#### 3.1. Milled end-product structure as a function of the initial composition

Table 3 lists the end-product compositions and the related structures as a function of the initial mean composition corresponding to the P5/2(10) milling conditions and an initial mixture of elemental iron and silicon powders. Table 4 lists the end-product corresponding to the same milling conditions for an initial state corresponding to melt-spun ribbons. The experimental XRD patterns and the corresponding APD and ABFfit deconvolution results are available by writing directly to the authors.

##### 3.1.1. $0 < Si$ (wt.%) $< 16$

In this composition range, a mixture of a crystalline b.c.c. phase and an amorphous phase is observed by XRD pattern analyses. According to Fig. 1 which presents the equilibrium Fe–Si phase diagram, it is worth noting that the domain corresponding to the crystalline b.c.c. Fe(Si) has been considerably enlarged: up to 16 wt.% silicon. The end product corresponding to the various initial states (*i.e.* a mixture of the elemental

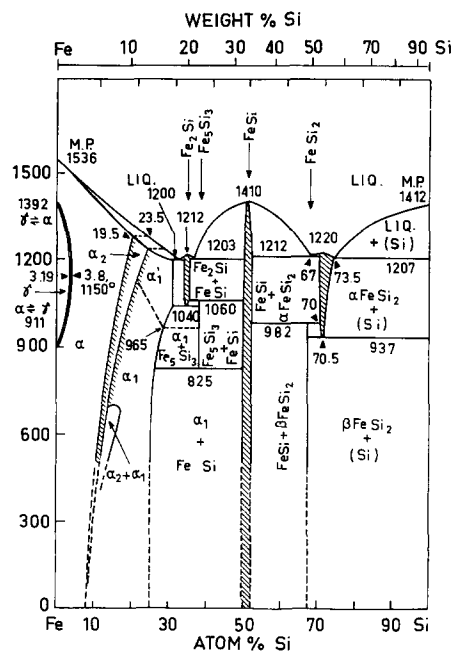


Fig. 1. Fe–Si equilibrium phase diagram (from ref. 171).

components or pieces of melt-spun ribbons corresponding to a composition equal to 10 wt.% silicon) are identical.

##### 3.1.2. $17 \leq Si$ (wt.%) $\leq 50$

A mixture of distinct crystalline phases and an amorphous phase(s) was detected (see Table 3). The presence of the metastable phase (at least at room temperature)  $\eta$ -Fe<sub>5</sub>Si<sub>3</sub> is observed.

Furthermore, it is worth noting that silicon depletion is detected in the initial silicon composition range 30–50 wt.%. This depletion is observed for both initial states (a mixture of elemental powder or melt-spun ribbons).

The position of the diffuse halo which is related to the presence of the amorphous phase corresponds to the crystalline peak position of some crystalline phases. Therefore, the composition of the amorphous phase was assumed to correspond to that of the related crystalline phase.

##### 3.1.3. $50 \leq Si$ (wt.%) $< 100$

The structure of the end product essentially corresponds to a mixture of the crystalline metastable  $\alpha$ -FeSi<sub>2</sub> and crystalline silicon phases added to an amorphous phase. As observed in Table 3, in some cases the crystalline FeSi (initial silicon content equal to 90 wt.%) or  $\beta$ -FeSi<sub>2</sub> (initial silicon content equal to 70 wt.%) compounds may be detected. In the case of the melt-spun ribbons, destabilization of the initial (silicon,  $\beta$ -FeSi<sub>2</sub>) phase mixture occurs leading to an end-product corresponding to a mixture of the silicon and  $\alpha$ -FeSi<sub>2</sub> phases (see Table 4).

### 3.2. Supersaturated Fe(Si) phase formation by mechanical alloying

#### 3.2.1. Crystalline lattice parameter and grain size as a function of the milling duration

Figures 2–4 exhibit the crystalline lattice parameter, the ranges of grain size as well as the grain size lattice parameter as a function of the milling duration and the initial composition corresponding to the formation of MA amorphous and crystalline Fe(Si) phases. The figures detail the results which are listed in Table 5.

From these figures, one may observe the following.

The silicon content in the crystalline Fe(Si) phase increases as the MA process evolves. Indeed, after 12 h, some silicon crystalline peak contributions are observed on the XRD patterns, but no crystalline silicon peak remains after 24 h.

Amorphization may occur before the complete dissolution of silicon into the iron crystalline lattice.

The grain sizes decrease as a function of the milling duration (Fig. 4(b)).

The milling process induces an expansion of the crystalline lattice parameter compared with the corresponding equilibrium Fe(Si) phase (Fig. 2).

As the milling duration increases, the silicon content inside the Fe(Si) crystalline phase increases leading to a decrease in the lattice parameter (Fig. 4(a)).

For the shortest milling duration (12 h), and for a given initial concentration, the lower the crystalline lattice parameters, the lower the crystalline grain sizes (Fig. 3(a)).

For the longest milling durations (24, 168 h), for a given initial concentration (with the exception of the compositions equal to 16 wt.% (24 h) and 15 wt.% (168 h) – this exception will be discussed below), the larger the crystalline lattice parameters, the smaller the grain sizes and *vice versa* (Figs. 3(b) and 3(c)).

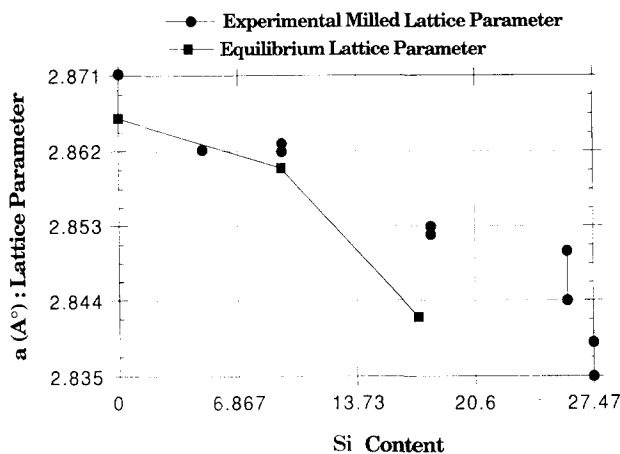


Fig. 2. Lattice parameter corresponding to the crystalline b.c.c. Fe(Si) phase: ■ thermal equilibrium phase (from ref. 172), ● mechanical alloyed crystalline Fe(Si) phase. (The silicon concentration is expressed in atomic per cent.)

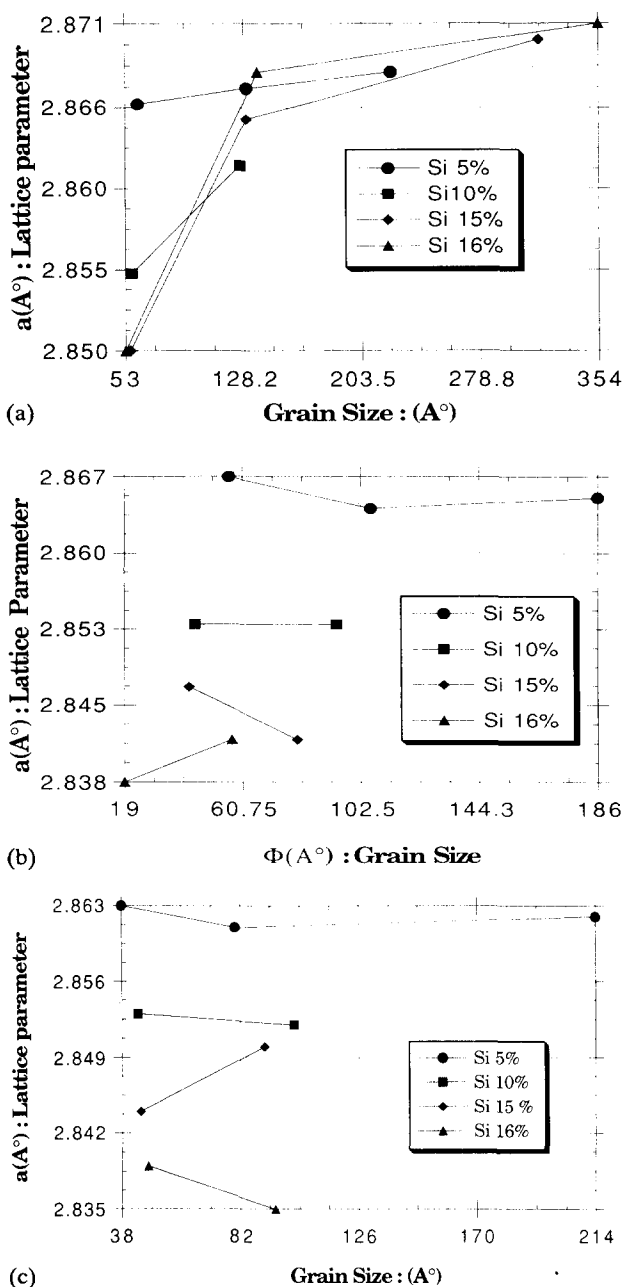


Fig. 3. Lattice parameter corresponding to the crystalline b.c.c. Fe(Si) phase as a function of class of grain size after 12 (a), 24 (b), and 168 (c) h of MA starting from a mixture of the elemental components. (The silicon concentration is expressed in weight per cent.)

#### 3.2.2. Mechanism of the Fe(Si) crystalline to amorphous phase transition

(i) For the shortest milling duration (12 h), the experimental results show that the lower the crystalline lattice parameter is, the lower is the crystalline grain size. For a silicon content of 5 wt.%, the ductility of the crystalline Fe(Si) phase is zero (at least at room temperature) [172]. Therefore, during the initial stages of the milling process, the iron grains into which the silicon atoms enter become brittle, leading to a decrease

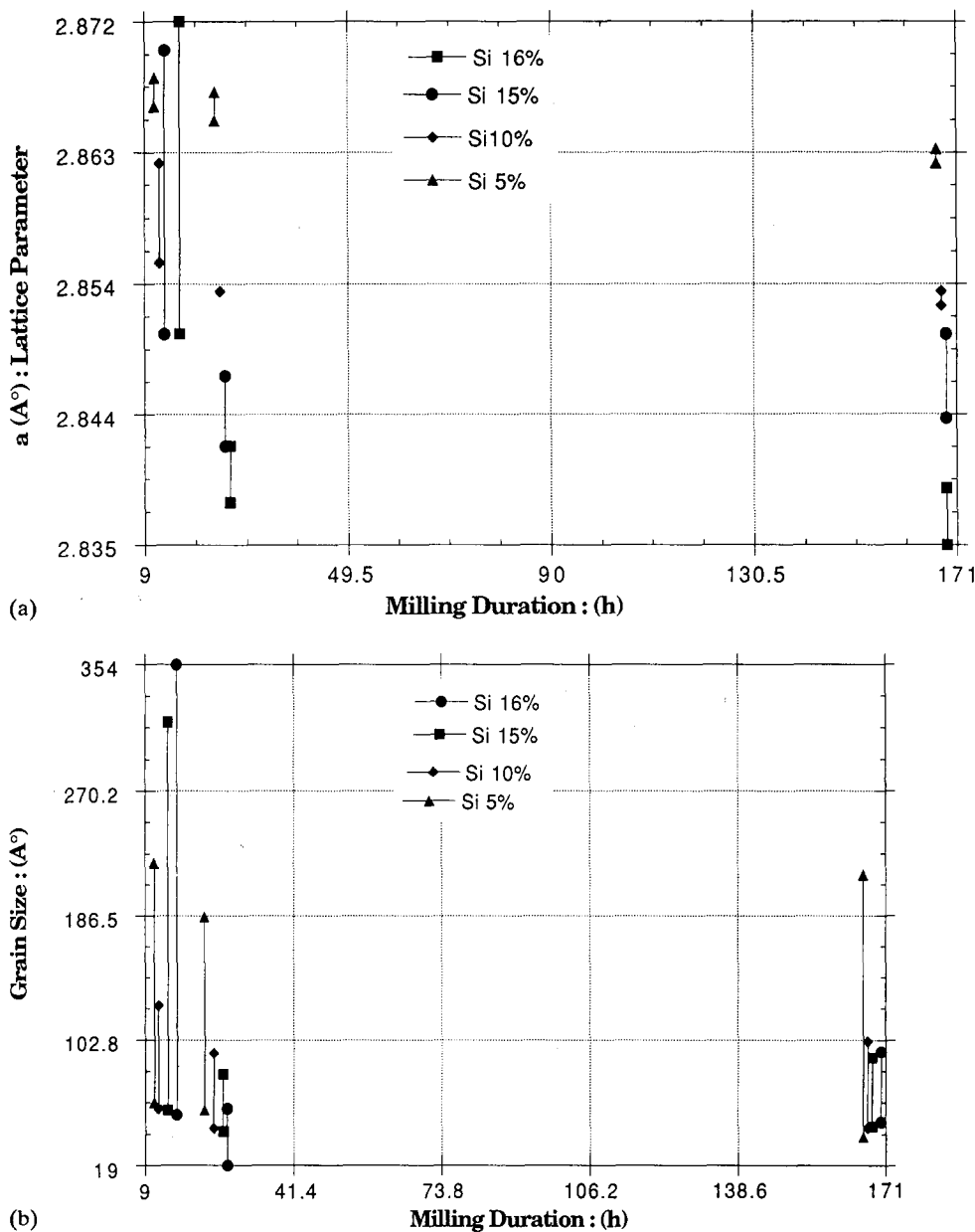


Fig. 4. Evolution of (a) lattice parameter and (b) grain size classes corresponding to the crystalline C.C. Fe(Si) phase as a function of the initial composition (expressed in weight per cent) starting from a mixture of the elemental components.

in their size range. Thus, owing to the inhomogeneity of the milling process at the beginning, partition of the iron grains is observed (the grains corresponding to the largest silicon content exhibit the smallest size, while those corresponding to the lowest silicon content exhibit the largest grain size). Furthermore, grains with the largest silicon content exhibit the lowest lattice parameter. These results are observed in the XRD patterns corresponding to 12 h milling duration.

(2) For the longest milling durations (24, 168 h), the larger the crystalline lattice parameter is, the smaller is the grain size (and *vice versa*). For such long milling durations and for a given initial concentration, the silicon atoms are assumed to be homogeneously dis-

tributed inside the crystalline iron grains. In other words, the lattice parameter should statistically be the same. It is worth emphasizing that the higher the initial silicon content, the lower the value of crystalline Fe(Si) lattice parameter. This observation is in agreement with the results reported by Tenwick and Davies [172] who reported on the formation of rapidly solidified Fe-Si alloy.

Nevertheless, taking into account the experimental results which show that the longest milling durations produce the lowest grain size and the highest lattice parameter (and *vice-versa*), one may propose that the effects of the milling process (*i.e.* the shock efficacy) are not well distributed: some of the grains have been

TABLE 5. End-product structure as a function of the milling duration (12, 24 and 168 h)

The chosen compositions correspond to the supersaturated Fe(Si) domain. It is worth noting that for the milling duration of 12 h and for all the investigated compositions, some silicon crystalline phase traces were detected by the presence of the corresponding XRD peak contributions

Initial composition, Si content (wt.%)	Milling duration (h)	Grain size (nm)	Crystalline lattice parameter (nm)	Amorphous peak position $d$ (nm)
5	12	$6.1 \leq \Phi \leq 22.2$	$0.2867 \pm 0.0001$	0.1999
5	24	$5.6 \leq \Phi \leq 18.6$	$0.2865 \pm 0.0002$	0.2000
5	168	$3.8 \leq \Phi \leq 21.4$	$0.2862 \pm 0.0001$	0.1997
10	12	$5.7 \leq \Phi \leq 12.6$	$0.2859 \pm 0.0004$	0.1991
10	24	$4.4 \leq \Phi \leq 9.4$	$0.2853 \pm 0.0001$	0.1998
10	168	$4.4 \leq \Phi \leq 10.2$	$0.2852 \pm 0.0001$	0.2012
15	12	$5.6 \leq \Phi \leq 31.6$	$0.2865 \pm 0.0015$	0.1989
15	24	$4.2 \leq \Phi \leq 8.0$	$0.2845 \pm 0.0003$	0.2009
15	168	$4.5 \leq \Phi \leq 9.1$	$0.2847 \pm 0.0003$	0.2007
16	12	$5.3 \leq \Phi \leq 35.4$	$0.2863 \pm 0.0013$	0.1984
16	24	$1.9 \leq \Phi \leq 5.7$	$0.2840 \pm 0.0002$	0.1995
16	168	$4.8 \leq \Phi < 9.5$	$0.2837 \pm 0.0002$	0.2011

submitted to a larger number of shocks than others. Therefore, owing to the brittleness of the crystalline Fe(Si) lattice, the inhomogeneity of the shock process leads to a stronger refinement of the former grains than of the latter.

Based on our previous work on the crystalline to amorphous phase transition induced by ball-milling in the pure silicon and germanium systems [99, 155], one may propose that the refinement of the crystalline Fe(Si) grains leads to a lattice expansion as the milling process evolves. This can also explain Fig. 2 which shows that the lattice parameter of the Fe(Si) crystalline phase obtained by MA is larger than the corresponding value obtained under equilibrium thermodynamic conditions [172]. Therefore, the expansion of the lattice parameter due to a critical refinement of the crystalline grain explains the observations of long milling duration experiments, *i.e.* the lower the crystalline grain size, the higher the value of the lattice parameter.

The expansion of the lattice parameter was explained previously as being a method of compensating for the surface energy by a volume energy. Indeed, the surface energy becomes the dominant factor when the lattice grain size reaches a critical value. Furthermore, the lattice expansion may explain the supersaturated crystalline Fe(Si) phase domain. Such an effect of the lattice expansion on the existence of a supersaturated crystalline phase domain has been previously reported in our work on the crystalline to amorphous phase transition induced by MA in the immiscible Si–Sn and Si–Zn systems [157].

As the milling process evolves, the continuous refinement of the crystalline grain which is accompanied by silicon supersaturation is no longer compensated for by a lattice expansion. Therefore, as the crystalline phase grains reach a critical value, the crystalline phase

becomes unstable and the amorphous phase forms.

Furthermore, it is worth noting that the position of the amorphous peak does not change as a function of the milling duration and that the ratio of the intensity of the crystalline [110] Fe(Si) peak to the first amorphous halo intensity decreases from 12 to 168 h. That means that the crystalline to amorphous phase transition is a polymorphous phase transition.

It is worth noting that for the silicon content corresponding to the limit of composition of the crystalline Fe(Si) phase domain (*i.e.* 15–16 wt.%) and for long milling durations (168 and 24 h respectively), the effect of inhomogeneity of the milling process may explain the apparent particular relation between the grain size and the lattice parameter: the lower the grain size, the lower the lattice parameter value. This inhomogeneity is well reinforced by the fact that the concentrations concerned correspond to the limits of the Fe(Si) domain.

### 3.3. Structure of the end-product as a function of milling conditions and annealing temperature for the initial $Fe_{33.3}Si_{66.6}$ (At.%) composition

Table 6 lists the results of the as-mechanically milled powder corresponding to the initial composition  $Fe_{33.3}Si_{66.6}$  (expressed in atomic per cent). The short milling durations were chosen to obtain a large mixture of the initial iron and silicon phases. Nevertheless, according to the reported results, it is worth noting that the  $\alpha$ -FeSi<sub>2</sub> and FeSi phases have formed during this process of short duration.

#### 3.3.1. As-mechanically milled end-product for the initial composition $Fe_{33.3}Si_{66.6}$ (at.%)

As mentioned above, the end-product phases corresponding to the various chosen energetic milling conditions are reported in Table 6.

TABLE 6. End-product structure as a function of the mechanical conditions and the isothermal annealing temperature corresponding to the initial composition  $\text{Fe}_{33.3}\text{Si}_{66.6}$  (at.-%), and the  $G7(\Omega/\omega/\Delta t)$  milling conditions, determination of the end-product silicon content (EDX-SEM analyses) and identification of the end-product structure (XRD patterns)

The major phases detected are noted \*\*.

$\Omega/\omega/\Delta t$ (rev min <sup>-1</sup> / rev min <sup>-1</sup> h)	End-product Si content (at.-%)	As mechanically milled phases	24 h, 300 °C	24 h, 500 °C	24 h, 800 °C
700/250/1	31.5±1.0	Fe+Si+ $\alpha$ -FeSi <sub>2</sub> +FeSi +amorphous phase (0.304)	Fe**+Si**+ $\alpha$ -FeSi <sub>2</sub> +FeSi	$\beta$ -FeSi <sub>2</sub> **+Si+Fe +FeSi(-)+Fe <sub>3</sub> Si(-)+ $\eta$ -Fe <sub>5</sub> Si <sub>3</sub> (-)+X(?) +amorphous phase (1.89)	$\beta$ -FeSi <sub>2</sub> **+FeSi <sub>2</sub> + $\alpha$ -FeSi <sub>2</sub> (-)+X(?)
700/250/2	33.6±1.0	Fe**+Si**+ $\alpha$ -FeSi <sub>2</sub> +FeSi +amorphous phase (0.314)	Fe**+Si**+FeSi + $\alpha$ -FeSi <sub>2</sub>	$\beta$ -FeSi <sub>2</sub> **+FeSi+ $\alpha$ -FeSi <sub>2</sub> +X(?)	$\beta$ -FeSi <sub>2</sub> **+Si+Fe +X(?)
700/250/3	33.0±1.0	Fe**+ $\alpha$ -FeSi <sub>2</sub> **+FeSi+Si +amorphous phase (0.188)	$\alpha$ -FeSi <sub>2</sub> **+FeSi + $\beta$ -FeSi <sub>2</sub> (-)	FeSi**+ $\beta$ -FeSi <sub>2</sub> + $\alpha$ -FeSi <sub>2</sub> +Fe+Si+X(?)	FeSi**+Si+ $\beta$ -FeSi <sub>2</sub> +Fe <sub>3</sub> Si+X(?)
600/250/1	25.6±2.0	Fe**+Si**+amorphous phase (0.314)	Fe**+Si**	$\alpha$ -FeSi <sub>2</sub> **+FeSi + $\beta$ -FeSi <sub>2</sub> (-)+Si(-)+X(?) +amorphous phase (1.85)	$\beta$ -FeSi <sub>2</sub> **+FeSi+ $\alpha$ -FeSi <sub>2</sub> + $\eta$ -Fe <sub>5</sub> Si <sub>3</sub> +X(?)
600/250/2	35.5±0.7	Fe**+Si**+ $\alpha$ -FeSi <sub>2</sub> (-) +amorphous phase (0.316)	Fe**+Si**+FeSi <sub>2</sub> + $\alpha$ -FeSi <sub>2</sub>	$\alpha$ -FeSi <sub>2</sub> **+FeSi+ $\beta$ -FeSi <sub>2</sub> +X(?)	$\beta$ -FeSi <sub>2</sub> **+FeSi+ $\alpha$ -FeSi <sub>2</sub> +Si+ $\eta$ -Fe <sub>5</sub> Si <sub>3</sub> (-)
600/250/3	35.0±0.6	Fe**+Si**+ $\alpha$ -FeSi <sub>2</sub> +amorphous phase (0.315)	Fe**+Si**+FeSi <sub>2</sub> + $\alpha$ -FeSi <sub>2</sub>	Fe**+Si**+FeSi +amorphous phase (0.310)	FeSi**+ $\beta$ -FeSi <sub>2</sub> +Si + $\alpha$ -FeSi <sub>2</sub> (-)+X(?)
500/250/2	29.5±0.7	Fe**+Si**	Fe**+Si**+FeSi +amorphous phase (0.310)	FeSi**+FeSi <sub>2</sub> *+Si* + $\beta$ -FeSi <sub>2</sub> (-)+X(?)	$\alpha$ -FeSi <sub>2</sub> **+FeSi <sub>2</sub> + $\alpha$ -FeSi <sub>2</sub> (-)+X(?)
500/250/3	32.2±1.0	Fe**+Si**	Fe**+Si**+FeSi +amorphous phase (0.315)	FeSi**+FeSi <sub>2</sub> *+Si* + $\beta$ -FeSi <sub>2</sub> (-)+X(?)	$\beta$ -FeSi <sub>2</sub> **+FeSi+ $\alpha$ -FeSi <sub>2</sub> +Fe+Si+X(?)
500/250/6	34.4±1.8	Fe**+Si**+FeSi <sub>2</sub> + $\alpha$ -FeSi <sub>2</sub>	Fe**+Si**+FeSi + $\alpha$ -FeSi <sub>2</sub>	FeSi**+ $\beta$ -FeSi <sub>2</sub> +Si+X(?)	$\beta$ -FeSi <sub>2</sub> +FeSi+ $\alpha$ -FeSi <sub>2</sub> +Fe+Si+X(?)

**Crystalline phases.** In the case of the highest energy milling conditions (*i.e.*  $\Omega = 700 \text{ rev min}^{-1}$ ) and for all process durations (*i.e.* 1, 2, 3 h), the end-product corresponds to a mixture of the iron, silicon, FeSi and  $\alpha\text{-FeSi}_2$  crystalline phases added to an amorphous phase. The presence of crystalline phases which are distinct from the elemental phases is observed for the milling processes corresponding to the lower energetic conditions but for longer milling durations.

Furthermore, particular attention should be paid to the  $\alpha\text{-FeSi}_2$  phase formation induced by ball-milling. Indeed, this phase formation is observed under thermodynamic equilibrium conditions for temperatures higher than 967 °C (Fig. 1): the  $\beta\text{-FeSi}_2$  phase decomposes peritectoidally into the FeSi and  $\alpha\text{-FeSi}_2$  phases above 967 °C. No trace of  $\beta\text{-FeSi}_2$  was detected in the XRD patterns.

Further, more detailed APD deconvolution analyses of the XRD patterns lead to determination of the iron and silicon grain sizes, as well as the iron and silicon lattice parameter and the crystalline lattice strains corresponding to the as-milled powders (Table 7).

**Amorphous phases.** Two types of amorphous phase were observed: one corresponding to a  $(0.310 \pm 0.006 \text{ nm})$  first halo position, the other corresponding to a 0.188 nm amorphous peak position. The first phase may be assumed to correspond to an amorphous silicon based phase. Indeed, such an amorphous phase has been detected in our previous work [155] which deals with the crystalline to amorphous phase transition induced by ball-milling of pure silicon powder. The amorphization transition was attributed to a lattice instability

which is the consequence of a decrease in grain size accompanied by expansion of the lattice parameter.

### 3.3.2. Structure corresponding to a 300 °C 24 h isothermal anneal

Table 8 details the results which are listed in Table 6. It is worth noting that the same deconvolution conditions were chosen for the APD XRD pattern analyses. In other words, no artefact has been introduced by such a method and direct comparison is possible between the results corresponding to the as-milled and the 300 °C isothermal annealed structures.

The major effect of the annealing is that both the iron and silicon crystalline phases exhibit a larger range of grain size than the as-milled powders. Indeed, to analyse the [111] silicon and the [110] iron peaks, two crystalline contributions are required to fit each peak.

### 3.3.3. Structure corresponding to a 500 °C 24 h isothermal anneal

**$\beta\text{-FeSi}_2$  phase.** For all the investigated milling conditions, the major effects of a 500 °C isothermal annealing process occurring during 24 h are the formation of the  $\beta\text{-FeSi}_2$  phase and the decrease in the fractions of elemental iron and silicon phases. The  $\beta\text{-FeSi}_2$  phase is the major phase formed for the 500 °C annealed (700/250/1, 2, 3, h) and (500/250/6 h) milled powders. However, it is worth noting that the  $\alpha\text{-FeSi}_2$  phase is the major phase formed for the 500 °C annealed (600/250/2, 3 h) and (500/250/2, 3 h) milled powders.

**Amorphous phase (700/250/1 h, 600/250/2 h).** It is worth noting that for the just reported MA conditions, 500 °C isothermal annealing leads to the formation of

TABLE 7. Determination of the silicon and iron lattice parameters, grain sizes and lattice strains corresponding to the as-milled powders

$\Omega/\omega/\Delta t$ (rev min <sup>-1</sup> / rev min <sup>-1</sup> /h)	Si lattice parameter (nm)	Si grain size (nm)	Si strain	Fe lattice parameter (nm)	Fe grain size (nm)	Fe strain
700/250/1	0.5443	34.6	0.701	0.2869	42.0	0.355
700/250/2	0.5453	31.0	1.031	0.2869	31.9	0.560
700/250/3	0.5315	11.6	—	0.2839	18.8	0.745
600/250/1	0.5442	127.4 <sup>a</sup>	0.403	0.2870	169.0*	0.267
600/250/2	0.5442	39.2	0.603	0.2870	58.2	0.295
600/250/3	0.5436	20.9	0.964	0.2869	46.7	0.356
500/250/2	0.5432	46.5	0.564	0.2867	75.0	0.307
500/250/3	0.5421	18.6	1.36	0.2866	71.8	0.328
	0.5428	127.4 <sup>a</sup>	0.313			
500/250/6	0.5433	48.4	0.532	0.2868	71.8	0.239
250/250/2	0.5445	132.3 <sup>a</sup>	0.277	0.2871	160.0 <sup>a</sup>	0.240
250/250/3	0.5443	197.9 <sup>a</sup>	0.236	0.2870	21.0	0.256
250/250/6	0.5441	132.3 <sup>a</sup>	0.277	0.2870	208.1 <sup>a</sup>	0.239

\*Owing to the instrumental width of the diffraction peak (which corresponds to an equivalent grain size of about 100–500 nm), the results of APD which lead to determination of a grain size of more than 500 nm have no physical significance.

TABLE 8. Determination of the silicon and iron lattice parameters, grain sizes and lattice strains corresponding to the 300 °C isothermally annealed MA powders

$\Omega/\omega/\Delta t$ (rev min <sup>-1</sup> / rev min <sup>-1</sup> /h)	Si lattice parameter (nm)	Si grain size (nm)	Si strain	Fe lattice parameter (nm)	Fe grain size (nm)	Fe strain
700/250/1	0.5440	174.7 <sup>a</sup>	0.332	0.2870	282.2 <sup>a</sup>	0.219
	0.5441	24.3	1.164	0.2839	33.4	0.524
700/250/2	0.5446	341.9 <sup>a</sup>	0.422	0.2860	10.6	1.618
	0.5448	22.8	1.268	0.2873	703.2 <sup>a</sup>	0.233
700/250/3	No more Si phase	—	—	No more Fe phase	—	—
600/250/1	0.5447	211.8 <sup>a</sup>	0.394	0.2872	4077.1 <sup>a</sup>	0.162
				0.2848	29.8	0.657
				0.2874	146.0 <sup>a</sup>	0.252
600/250/2	0.5444	177.5 <sup>a</sup>	0.411	0.2872	202.2	0.225
	0.5446	18.2	1.910	0.2839	31.5	0.448
600/250/3	0.5414	44.1	0.574	0.2863	254.6 <sup>a</sup>	0.239
	0.5409	8.4	2.846			
500/250/2	0.5441	51.4	0.150	0.2871	3011.4 <sup>a</sup>	0.220
	0.5439	15.4	0.855	0.2847	28.0	0.832
500/250/3	0.5440	57.6	0.139	0.2870	820.7 <sup>a</sup>	0.222
	0.5437	17.0	0.762	0.2847	15.5	0.730
500/250/6	0.5450	46.1	0.857	0.2873	653.7 <sup>a</sup>	0.216
				0.2844	31.7	0.706

<sup>a</sup>Owing to the instrumental width of the diffraction peak (which corresponds to an equivalent grain size of about 100–500 nm), the results of APD which lead to determination of a grain size of more than 500 nm have no physical significance.

an amorphous phase for which the first diffuse halo corresponds to a  $d$  value equal to  $0.187 \pm 0.002$  nm. Therefore this experimental result can be compared with what happens in the case of solid state amorphization induced by diffusion starting from a multilayer system. Amorphization induced by annealing has been reported previously for the Ti/Si [173–175], Rh/Si [176], and Zr/Si [177] multilayer systems. To our knowledge, this is the first time that such an amorphization induced by post-milling annealing has been reported in the Fe–Si system.

### 3.3.4. Structure corresponding to an 800 °C 24 h isothermal anneal

*Decrease in  $\alpha$ -FeSi<sub>2</sub>.* For all the investigated milling conditions, the 800 °C isothermal annealing process leads to a decrease in the  $\alpha$ -FeSi<sub>2</sub> content. In particular cases (700/250/3 h, 600/250/1 h), no more trace of such a phase was observed.

*FeSi,  $\beta$ -FeSi<sub>2</sub>, silicon end-product.* In fact, according to the results listed in Table 6, the end product corresponding to an 800 °C isothermal annealing process tends to correspond to a mixture of FeSi,  $\beta$ -FeSi<sub>2</sub> and silicon crystalline phases.

## 4. Conclusion

Based on X-ray diffraction patterns, the structures of end-products corresponding to far from equilibrium phase transitions induced by mechanical alloying and post-milling isothermal annealing in the Fe–Si system have been characterized.

(i) *As milled powder.* For an initial powder composition corresponding to the iron-rich side of the (Fe, Si) phase diagram, the major result of the study related to the influence of the composition on the P5/2(10) milled powder is the possibility of expanding the solubility limit of silicon in the crystalline Fe(Si) phase up to 16 wt.%. Furthermore, in this related composition range the crystalline to amorphous phase formation corresponds to a polymorphous phase transition. For an initial composition located in the silicon-rich side of the phase diagram, it is worth noting that the chosen milling conditions lead to the formation of the metastable high temperature  $\alpha$ -FeSi<sub>2</sub> phase instead of the stable  $\beta$ -FeSi<sub>2</sub> phase. Furthermore, in the case of the melt-spun ribbons for which the initial state corresponds to a phase mixture containing the  $\beta$ -FeSi<sub>2</sub> phase, destabilization of this phase is observed.

(ii) *Post milling annealed powder.* The structure related to the as-milled Fe<sub>33.3</sub>Si<sub>66.6</sub> (at.%) composition corre-

sponds to an iron, silicon, FeSi and  $\alpha$ -FeSi<sub>2</sub> crystalline phase mixture added to an amorphous phase. The annealing firstly leads to the disappearance of the iron phase and of the metastable crystalline  $\alpha$ -FeSi<sub>2</sub> compound, as well as the amorphous phase which was formed during the milling process, and secondly leads to the formation of the  $\beta$ -FeSi<sub>2</sub> phase. Therefore, the end-product of isothermal annealing tends to be a mixture of FeSi,  $\beta$ -FeSi<sub>2</sub> and silicon phases. Another interesting feature is the fact that under specific milling conditions, a 500 °C isothermal anneal of short duration of MA (Fe, Si) powders leads to the formation of an amorphous phase.

## Acknowledgments

The author thanks the workshop staff (CECM-CNRS) for the design and realization of the special G7 high energy planetary ball-milling system.

## References

- 1 A. E. Yermakov, E. E. Yurchikov and V. A. Barinov, *Fiz. Met. Metalloved.*, 52 (1981) 1184.
- 2 A. E. Yermakov, E. E. Yurchikov and V. A. Barinov, *Phys. Met. Metall.*, 52(6) (1981) 50–58.
- 3 C. C. Koch, O. B. Cavin, C. G. McKamey and J. O. Scarbrough, *Appl. Phys. Lett.*, 43(11) (1983) 1017–1019.
- 4 J. S. Benjamin, *Metall. Trans.*, I(1970) 2943.
- 5 J. S. Benjamin and R. D. Schelleng, *Metall. Trans A*, 12 (1981) 1827.
- 6 J. S. Benjamin and M. J. Bomford, *Metall. Trans. A*, 8 (1977) 1301.
- 7 J. S. Benjamin and T. E. Volin, *Metall. Trans.*, 5 (1974) 1929.
- 8 T. G. Richards and G. P. Johari, *Philos. Mag.*, 58B(4) (1988) 445.
- 9 P. I. Loeff and H. Bakker, *Europhys. Lett.*, 8(1) (1989) 35–40.
- 10 H. Bakker, P. I. Loeff and A. W. Weeber, *Defect Diffus. Forum*, 66–69 (1989) 1169–1186.
- 11 P. H. Shingu, B. Huang, J. Kuyama, K. N. Ishihara and S. Nasu, in E. Arzt and L. Schultz (eds.), *Proc. DGM Int. Conf. on New Materials by Mechanical Alloying Techniques*, Calw-Hirsau, October 1988, Deutsche Gesellschaft für Metallkunde, Informationsgesellschaft, Düsseldorf, 1989, pp. 319–326.
- 12 T. Tsuchida and K. Sugimoto, *Thermochim. Acta*, 170 (1990) 41–50.
- 13 A. Eckert, L. Schultz and B. Urban, *Europhys. Lett.*, 13(4) (1990) 349–354.
- 14 J. Eckert, L. Schultz and K. Urban, *J. Less-Common Met.*, 167 (1990) 143–152.
- 15 G. B. Schaffer and P. G. McCormick, *J. Mater. Sci. Lett.*, 9 (1990) 1014–1016.
- 16 Y. D. Dong, W. H. Wang, L. Liu, K. Q. Xiao, S. H. Tong and Y. Z. He, in H. Fredriksson and S. Savage (eds.), *Proc. 7th Int. Conf. on Rapidly Quenched Metals*, Stockholm, August 1990, in *Mater. Sci. Eng.*, A134 (1991) 867–871.
- 17 B. Huang, N. Tokizane, K. N. Ishihara, P. H. Shingu and S. Nasu, *J. Non-Cryst. Solids*, 117–118 (1990) 688–691.
- 18 P. H. Shingu, B. Huang, S. R. Nishitani and S. Nasu, *Proc. JIMIS 5: Non Equilibrium Phase Metals and Alloys*, Suppl. Trans. JIM, 29 (1988) 3–10.
- 19 D. G. Morris and M. A. Morris, *Mater. Sci. Eng.*, A125 (1990) 97–106.
- 20 J. M. Papazian and P. Gilman, *Mater. Sci. Eng.*, A125 (1990) 121–127.
- 21 E. Hellstern, L. Schultz, R. Bormann and D. Lee, *Appl. Phys. Lett.*, 53(15) (1988) 1399–1401.
- 22 M. Oehring and R. Bormann, in A. R. Yavari and P. J. Desré (eds.), *Proc. Int. Symp. on Solid State Reaction*, Grenoble, February 1990, in *J. Phys., Coll. Phys. C4, Suppl.* 14, 51 (1990) 169.
- 23 M. Oehring and R. Bormann, in H. Fredriksson and S. Savage (eds.), *Proc. 7th Int. Conf. on Rapidly Quenched Metals*, Stockholm, August 1990, in *Mater. Sci. Eng.*, A134 (1991) 1330–1333.
- 24 G. Cocco, S. Enzo, L. Schiffini and L. Battezzati, in E. Arzt and L. Schultz (eds.), *Proc. DGM Int. Conf. on New Materials by Mechanical Alloying Techniques*, Calw-Hirsau, October 1988, Deutsche Gesellschaft für Metallkunde, Informationsgesellschaft, Düsseldorf, 1989, pp. 343–348.
- 25 C. C. Koch, J. S. C. Jang and P. Y. Lee, in E. Arzt and L. S. Schultz (eds.), *Proc. DGM Int. Conf. on New Materials by Mechanical Alloying Techniques*, Calw-Hirsau, October 1988, Deutsche Gesellschaft für Metallkunde, Informationsgesellschaft, Düsseldorf, 1989, pp. 101–110.
- 26 C. C. Koch, *J. Non-Cryst. Solids*, 117–118 (1990) 670–678.
- 27 A. Calka and A. P. Radlinski, *Scripta Metall.*, 23 (1989) 1497–1502.
- 28 F. Bordeaux and R. Yavari, *J. Appl. Phys.*, 67(5) (1990) 2385.
- 29 E. Hellstern, H. J. Fecht, Z. Fu and W. L. Johnson, *J. Mater. Res.*, 4(6) (1989) 1292.
- 30 E. Hellstern, H. J. Fecht, Z. Fu and W. L. Johnson, *J. Appl. Phys.*, 65(1) (1989) 305.
- 31 M. S. El-Eskandarany, K. Aoki and K. Suzuki, *J. Less-Common Met.*, 167 (1990) 113–118.
- 32 M. S. El-Eskandarany, F. Itoh, K. Aoki and K. Suzuki, *J. Non-Cryst. Solids*, 117–118 (1990) 729–732.
- 33 G. Cocco, S. Enzo, L. Schiffini and L. Battezzati, *Mater. Sci. Eng.*, 97 (1988) 43–46.
- 34 G. Cocco, I. Soletta, L. Battezzati, M. Baricco and S. Enzo, *Philos. Mag.*, 61 (1990) 473–486.
- 35 R. Lerf and D. G. Morris, *Mater. Sci. Eng.*, A128 (1990) 119–127.
- 36 P. K. Mirchandani and R. C. Benn, in F. H. Froes and M. A. Cull (eds.), *Proc. 2nd Int. Conf. on SAMPE Metals and Metals Processing*, Dayton, OH, August 1988, Vol. 2, p. 188.
- 37 H. J. Fecht and W. L. Johnson, *J. Non-Cryst. Solids*, 117–118 (1990) 704–707.
- 38 E. Gaffet and J. P. Gaspard, in A. R. Yavari and P. J. Desré (eds.), *Proc. Int. Symp. on Solid State Reaction*, Grenoble, February 1990, in *J. Phys., Coll. Phys. C4, Suppl.* 14, 51 (1990) 205–210.
- 39 P. I. Loeff and H. Bakker, *Scripta Metall.*, 22 (1988) 401.
- 40 A. Corrias, G. Ennas, G. Licheri, G. Marongiu and G. Paschina, *Mater. Sci. Eng. A*, to be published. and *J. Mater. Sci.*, 26 (1991) 5081–5084.
- 41 A. Calka, A. P. Pogany, R. A. Shanks, H. Engelmann, *Mater. Sci. Eng.*, A128 (1990) 107–112.
- 42 M. A. Morris and D. G. Morris, in A. R. Yavari and P. J. Desré (eds.), *Proc. Int. Symp. on Solid State Reaction*, Grenoble, February 1990, in *J. Phys., Coll. Phys. C4, Suppl.* 14, 51 (1990) 211–217.

- 43 C. H. Lee, T. Fukunaga and U. Mizutani, in H. Fredriksson and S. Savage (eds.), *Proc. 7th Int. Conf. on Rapidly Quenched Metals, Stockholm, August 1990*, in *Mater. Sci. Eng.*, A134 (1991) 1334–1337.
- 44 A. P. Radlinski and A. Calka, in H. Fredriksson and S. Savage (eds.), *Proc. 7th Int. Conf. on Rapidly Quenched Metals, Stockholm, August 1990*, in *Mater. Sci. Eng.*, A134 (1991) 1376–1379.
- 45 D. E. Wittmer, S. J. Pierz and W. E. Brower, Jr., *J. Non-Cryst. Solids*, 116 (1990) 225–232.
- 46 L. Schultz, J. Wecker and E. Hellstern, *J. Appl. Phys.*, 61(8) (1987) 3583.
- 47 H. Miura, S. Isa and K. Omuro, *J. Non-Cryst. Solids*, 117–118 (1990) 741–744.
- 48 H.-R. Pak, J. Chu, R. J. Deangelis and K. Okazaki, *Mater. Sci. Eng.*, A118 (1989) 147–153.
- 49 A. Calka and A. P. Radlinski, *J. Less-Common Met.*, 161 (1990) L23–L26.
- 50 E. Batalla and E. G. Zwart, *J. Mater. Res.*, 5(9) (1990) 1802.
- 51 K. Suzuki, *J. Non-Cryst. Solids*, 112 (1989) 23–32.
- 52 R. M. Davis, B. T. McDermott and C. C. Koch, *Metall. Trans. A*, 19 (1988) 2867.
- 53 H. Hashimoto and R. Watanabe, *Mater. Trans., JIM*, 31(3) (1990) 219.
- 54 G. LeCaér, P. Matteazzi, E. Bauer-Grosse, B. Fultz and A. Pianelli, in A. R. Yavari and P. J. Desré (eds.), *Proc. Int. Symp. on Solid State Reaction, Grenoble, February 1990*, in *J. Phys., Coll. Phys. C4, Suppl. 14, 51* (1990) 151–155.
- 55 J. Eckert, L. Schultz and K. Urban, *J. Less-Common Met.*, 166 (1990) 293–302.
- 56 D. Girardin and M. Maurer, in E. Arzt and L. Schultz (eds.), *Proc. DGM Int. Conf. on New Materials by Mechanical Alloying Techniques, Calw-Hirsau, October 1988*, Deutsche Gesellschaft für Metallkunde, Informationsgesellschaft, Düsseldorf, 1989, pp. 91–94.
- 57 A. E. Yermakov, E. E. Yurchikov and V. A. Barinov, *Fiz. Met. Metalloved.*, 54 (1982) 935.
- 58 H. Kimura, F. Takada and W.-N. Myung, *Mater. Sci. Eng.*, 97 (1988) 125–128.
- 59 M. Perret, H. Mehrer and N. A. Stolwijk, *Defect Diffus. Data*, 66–69 (1989) 1343–1348.
- 60 M. Schänzer and H. Mehrer, in A. R. Yavari and P. J. Desré (eds.), *Proc. Int. Symp. on Solid State Reaction, Grenoble, February 1990*, in *J. Phys., Coll. Phys. C4, Suppl. 14, 51* (1990) 87–93.
- 61 H. Kimura, *Solid State Phenom.*, 8–9 (1989) 47–60.
- 62 H. Kimura and F. Takada, *Mater. Sci. Eng.*, 97 (1988) 53.
- 63 M. Kimura, H. Kimura and T. Ban, *Proc. JIMIS-5, Kyoto, 1988*, p. 3.
- 64 A. Hikata, M. J. McKenna and C. Elbaum, *Appl. Phys. Lett.*, 50 (8) (1987) 478.
- 65 B. P. Dolgin, M. A. Vaneck, T. McGory and D. J. Ham, *J. Non-Cryst. Solids*, 87 (1986) 281–289.
- 66 E. Hellstern and L. Schultz, *Mater. Sci. Eng.*, 93 (1987) 213–216.
- 67 P. Y. Lee, J. Jang and C. C. Koch, *J. Less-Common Met.*, 140 (1988) 73–83.
- 68 E. Hellstern and L. Schultz, *Appl. Phys. Lett.*, 48(2) (1986) 124.
- 69 E. Hellstern and L. Schultz, *Philos. Mag. B*, 56(4) (1987) 443–448.
- 70 H. Kimura, M. Kimura and F. Takada, *J. Less-Common Met.*, 140 (1988) 113–118.
- 71 H. Kimura, *Proc. Sintering 89, Tokyo*, p. 89.
- 72 H. Kimura, M. Kimura and T. Ban, *Proc. 2nd Int. Conf. on Rapidly Solidified Materials Properties and Processing, San Diego, CA, March 7–9, 1988*, American Society for Metals, Metals Park, OH, 1988, p. 171.
- 73 A. W. Weeber and H. Bakker, *Z. Phys. Chem. N. F.*, 157 (1988) 221–225.
- 74 D. G. Morris and M. A. Morris, *Scripta Metall. Mater.*, 24 (1990) 1701–1706.
- 75 Y. Ogino, T. Yamasaki, S. Murayama and R. Sakai, *J. Non-Cryst. Solids*, 117–118 (1990) 737–740.
- 76 M. Atzman, K. M. Unruh and W. L. Johnson, *J. Appl. Phys.*, 58(10) (1985) 3865–3870.
- 77 J. R. Thompson, C. Politis and Y. C. Kim, in R. W. Cochrane and J. O. Ström-Olsen (eds.), *Proc. 6th Int. Conf. on Rapidly Quenched Metals, Montreal, August 1987*, in *Mater. Sci. Eng.*, 97 (1988) 31–34.
- 78 K. Matsuki, A. Inoue, H. M. Kimura and T. Masumoto, *Mater. Sci. Eng.*, 97 (1988) 47–51.
- 79 B. S. Murty, M. Mohan Rao and S. Ranganathan, *Scripta Metall. Mater.*, 24 (1990) 1819–1824.
- 80 T. Fukunaga, K. Nakamura, K. Suzuki and U. Mizutani, *J. Non-Cryst. Solids*, 117–118 (1990) 700–703.
- 81 K. Sakurai, Y. Yamada, C. H. Lee, T. Fukunaga and U. Mizutani, in H. Fredriksson and S. Savage (eds.), *Proc. 7th Int. Conf. on Rapidly Quenched Metals, Stockholm, August 1990*, in *Mater. Sci. Eng.*, A134 (1991) 1414–1417.
- 82 G. Cocco, I. Soletta, S. Enzo, M. Magini and N. Cowlam, in A. R. Yavari and P. J. Desré (eds.), *Proc. Int. Symp. on Solid State Reaction, Grenoble, February 1990*, in *J. Phys., Coll. Phys. C4, Suppl. 14, 51* (1990) 181–187.
- 83 G. Cocco, L. Schiffini, I. Soletta, S. Enzo, M. Baricco and N. Cowlam, in A. R. Yavari and P. J. Desré (eds.), *Proc. Int. Symp. on Solid State Reaction, Grenoble, February 1990*, in *J. Phys., Coll. Phys. C4, Suppl. 14, 51* (1990) 175–180.
- 84 C. Politis and W. L. Johnson, *J. Appl. Phys.*, 60 (3) (1986) 1147–1151.
- 85 T. Fukunaga, M. Mori, K. Inou and U. Mizutani, in H. Fredriksson and S. Savage (eds.), *Proc. 7th Int. Conf. on Rapidly Quenched Metals, Stockholm, August 1990*, in *Mater. Sci. Eng.*, A134 (1991) 863–866.
- 86 E. Gaffet, C. Louison, M. Harmelin and F. Faudot, in H. Fredriksson and S. Savage (eds.), *Proc. 7th Int. Conf. on Rapidly Quenched Metals, Stockholm, August 1990*, in *Mater. Sci. Eng.*, A134 (1991) 1380–1384.
- 87 B. T. McDermott and C. C. Koch, *Scripta Metall.*, 20 (1986) 669–672.
- 88 C. H. Lee, M. Mori and U. Mizutani, *J. Non-Cryst. Solids*, 117–118 (1990) 733–736.
- 89 S. Martelli, G. Mazzone, S. Scaglione and M. Vittori, *J. Less-Common Met.*, 145 (1988) 261.
- 90 M. Atzman, J. D. Verhoeven, E. D. Gibson and W. L. Johnson, *Appl. Phys. Lett.*, 45(10) (1984) 1052.
- 91 J. S. C. Jang and C. C. Koch, *Scripta Metall.*, 23 (1989) 1805–1810.
- 92 V. E. Martin, A. Garcia-Escorial, A. Martin, F. Carmona, F. Cebollada, P. Adeva and J. M. Gonzalez, in A. R. Yavari and P. J. Desré (eds.), *Proc. Int. Symp. on Solid State Reaction, Grenoble, February 1990*, in *J. Phys., Coll. Phys. C4, Suppl. 14, 51* (1990) 197–203.
- 93 L. Schultz, K. Schnitzke and J. Wecker, *Appl. Phys. Lett.*, 56(9) (1990) 868.
- 94 B. Fultz, G. Le Caér and P. Matteazzi, *J. Mater. Res.*, 4(6) (1989) 1450.

- 95 N. Burgio, A. Iasonna, M. Magini and F. Padella, in A. R. Yavari and P. J. Desré (eds.), *Proc. Int. Symp. on Solid State Reaction, Grenoble, February 1990*, in *J. Phys., Coll. Phys. C4, Suppl.* 14, 51 (1990) 265–271.
- 96 G. Ennas, M. Magini, G. Boffito and G. Licheri, *J. Mater. Sci.*, 24 (1989) 3053–3058.
- 97 E. Hellstern and L. Schultz, *J. Appl. Phys.*, 63(5) (1988) 1408–1413.
- 98 V. Michaelsen and E. Hellstern, *J. Appl. Phys.*, 62(1) (1987) 117–119.
- 99 E. Gaffet, *Mater. Sci. Eng.*, A136 (1991) 161–169.
- 100 E. A. Kenik, R. J. Bayuzick, M. S. Kim and C. C. Koch, *Scripta Metall.*, 21 (1987) 1137–1142.
- 101 M. S. Kim and C. C. Koch, *J. Appl. Phys.*, 62(8) (1987) 3450–3453.
- 102 J. S. C. Jang and C. C. Koch, *J. Mater. Res.*, 5(2) (1990) 325.
- 103 R. M. Davis and C. C. Koch, *Scripta Metall.*, 21 (1987) 305–310.
- 104 E. Gaffet, M. Harmelin and F. Faudot, *Mater. Sci. Eng.*, A149 (1991) 85–94.
- 105 C. C. Koch and J. S. C. Jang, *J. Mater. Res.*, 4(3) (1989) 557.
- 106 T. Ben Ameur and A. R. Yavari, in A. R. Yavari and P. J. Desré (eds.), *Proc. Int. Symp. on Solid State Reaction, Grenoble, February 1990*, in *J. Phys., Coll. Phys. C4, Suppl.* 14, 51 (1990) 219–226.
- 107 C. Suryanarayana and F. H. Froes, *J. Mater. Res.*, 5(9) (1990) 1880.
- 108 A. Calka and A. P. Radlinski, *Mater. Sci. Eng.*, A118 (1989) 131–135.
- 109 G. Cocco, S. Enzo, N. Barrett and K. J. Roberts, *J. Less-Common Met.*, 154 (1989) 177–186.
- 110 J. Y. Huot, M. L. Trudeau and R. Schulz, *J. Electrochem. Soc.*, 138 (1991) 1316.
- 111 F. Bordeaux, R. Yavari and P. Desré, in R. W. Cochrane and J. O. Ström-Olsen (eds.), *Proc. 6th Int. Conf. on Rapidly Quenched Metals, Montreal, August 1987*, in *Mater. Sci. Eng.*, 97 (1988) 129–132.
- 112 P. Y. Lee and C. C. Koch, *J. Non-Cryst. Solids*, 94 (1987) 88–100.
- 113 T. Nasu, K. Nagaoka, T. Sekiuchi, M. Sakurai, T. Fukunaga, F. Itoh and K. Suzuki, *J. Non-Cryst. Solids*, 117–118 (1990) 725–728.
- 114 F. Petzoldt, B. Scholz and H.-D. Kunze, *Modern Develop. Powder Metall.*, 18–21 (1988) 63.
- 115 F. Petzoldt, B. Scholz and H.-D. Kunze, *Mater. Lett.*, 5(7–8) (1987) 280.
- 116 L. M. Di, P. I. Loeff and H. Bakker, *Phys. Status Solidi A*, 117 (1990) K99.
- 117 T. J. Taininen and R. B. Schwarz, *J. Less-Common Met.*, 140 (1988) 99–112.
- 118 L. Battezzati, S. Enzo, L. Schiffini and G. Cocco, in K. Samwer, M. Von Allmen, J. Bottiger and B. Stritzker (eds.), *Proc. E-MRS, Strasbourg, May 31–June 2, 1988, Vol. 4*, 1988, p. 301.
- 119 L. Battezzati, G. Cocco, L. Schiffini and S. Enzo, *Mater. Sci. Eng.*, 97 (1988) 121–124.
- 120 M. S. Boldrick, D. Lee and C. N. J. Wagner, *J. Non-Cryst. Solids*, 106 (1988) 60–65.
- 121 S. Enzo, L. Schiffini, L. Battezzati and G. Coco, *J. Less-Common Met.*, 140 (1988) 129–137.
- 122 S. Enzo, L. Schiffini, L. Battezzati and G. Coco, *Mater. Sci. Eng.*, 97 (1988) 1450–1455.
- 123 J. Koike, D. M. Parkin and M. Nastasi, *J. Mater. Res.*, 5(7) (1990) 1414.
- 124 R. B. Schwarz, R. R. Petrich and C. K. Saw, *J. Non-Cryst. Solids*, 76 (1985) 281–302.
- 125 R. B. Schwarz and R. R. Petrich, *J. Less-Common Met.*, 140 (1988) 171–184.
- 126 R. B. Schwarz, *Mater. Sci. Eng.*, 97 (1988) 71–78.
- 127 B. E. White, M. E. Patt and E. J. Cotts, *Phys. Rev. B*, 42(17) (1990) 11017.
- 128 T. Fukunaga, Y. Homma, M. Misawa and U. Mizutani, *J. Non-Cryst. Solids*, 117–118 (1990) 721–724.
- 129 F. Bordeaux, E. Gaffet and R. Yavari, *Europhys. Lett.*, 12(1) (1990) 63–68.
- 130 A. Burbles and F. Petzoldt, *J. Non-Cryst. Solids*, 107 (1989) 233–238.
- 131 Y. Chen, R. Le Hazif and G. Martin, in A. R. Yavari and P. J. Desré (eds.), *Proc. Int. Symp. on Solid State Reaction, Grenoble, February 1990*, in *J. Phys., Coll. Phys. C4, Suppl.* 14, 51 (1990) 273–279.
- 132 J. Eckert, L. Schultz, E. Hellstern and K. Urban, *J. Appl. Phys.*, 64(6) (1988) 3224–3228.
- 133 E. Gaffet, N. Merk, G. Martin and J. Bigot, *J. Less-Common Met.*, 145 (1988) 251–260.
- E. Gaffet, N. Merk, G. Martin and J. Bigot, in E. Arzt and L. Schulz (eds.), *Proc. DGM Int. Conf. on New Materials by Mechanical Alloying Techniques, Calw-Hirsau, October 1988*, Deutsche Gesellschaft für Metallkunde, Informationsgesellschaft, Düsseldorf, 1989, pp. 98–100.
- 134 E. Gaffet, *Mater. Sci. Eng.*, A119 (1989) 185–197.
- 135 E. Gaffet, *Proc. E-MRS, Strasbourg, May 29–June 1, 1990; Symposium B, Metal Matrix Composites*, in *Mater. Sci. Eng.*, A135 (1991) 291–293.
- E. Gaffet, *Mater. Sci. Eng.*, A132 (1991) 181–193.
- 136 J. H. Harris, W. A. Curtin and L. Schultz, *J. Mater. Res.*, 3(5) (1988) 872.
- 137 J. Y. Huot, M. Trudeau, R. Schulz and A. Van Neste, *Int. J. Hydrogen Energy*, 15(4) (1990) 287–289.
- 138 P. Y. Lee and C. C. Koch, *J. Mater. Sci.*, 23 (1988) 2837–2845.
- 139 P. Y. Lee and C. C. Koch, *Appl. Phys. Lett.*, 50(22) (1987) 1578.
- 140 C. H. Lee, M. Mori, T. Fukunaga and U. Mizutani, *Jpn. J. Appl. Phys.*, 29(3) (1990) 540–544.
- 141 N. Merk, E. Gaffet and G. Martin, *J. Less-Common Met.*, 153 (1989) 299.
- 142 F. Petzoldt, B. Scholz and H.-D. Kunze, in R. W. Cochrane and J. O. Ström-Olsen (eds.), *Proc. 6th Int. Conf. on Rapidly Quenched Metals, Montreal, August 1987*, in *Mater. Sci. Eng.*, 97 (1988) 25–29.
- 143 F. Petzoldt, B. Scholz and H.-D. Kunze, *Mater. Sci. Eng.*, 97 (1989) 25–29.
- 144 F. Petzoldt, B. Scholz and H.-D. Kunze, in E. Arzt and L. Schulz (eds.), *Proc. DGM Int. Conf. on New Materials by Mechanical Alloying Techniques, Calw-Hirsau, October 1988*, Deutsche Gesellschaft für Metallkunde, Informationsgesellschaft, Düsseldorf, 1989, p. 111.
- 145 R. Schulz, M. Trudeau, J. Y. Huot and A. Van Neste, *Phys. Rev. Lett.*, 62(24) (1989) 2849.
- 146 R. Schulz, M. L. Trudeau and A. Van Neste, in H. Fredriksson and S. Savage (eds.), *Proc. 7th Int. Conf. on Rapidly Quenched Metals, August 1990*, in *Mater. Sci. Eng.*, A134 (1991) 1354–1360.
- 147 A. W. Weeber and H. Bakker, *J. Less-Common Met.*, 141 (1988) 93–102.
- 148 A. W. Weeber, H. Bakker, H. J. M. Heijligers and G. F. Bastin, *Europhys. Lett.*, 3(12) (1987) 1261–1265.
- 149 A. W. Weeber, W. J. Haag, A. J. H. Wester and H. Bakker, *J. Less-Common Met.*, 140 (1988) 119–127.

- 150 A. W. Weeber, H. Bakker and F. R. de Boer, *Europhys. Lett.*, 2(6) (1986) 445–448.
- 151 A. W. Weeber, K. Van der Meer, H. Bakker, F. R. de Boer, B. J. Thijssse and J. F. Jongste, *J. Phys. F*, 16 (1986) 1897–1904.
- 152 M. Magini, S. Martelli and M. Vittori, *J. Non-Cryst. Solids*, 101 (1988) 294–296.
- 153 J. R. Thompson and C. Politis, *Europhys. Lett.*, 3(2) (1987) 199–205.
- 154 P. I. Loeff, F. H. Spit and H. Bakker, *J. Less-Common Met.*, 145 (1988) 271–275.
- 155 E. Gaffet and M. Harmelin, *J. Less-Common Met.*, 157 (1990) 201–222.
- 156 G. Veltl, B. Scholz and H.-D. Kunze, in E. Arst and L. Schultz (eds.), *Proc. DGM Int. Conf. on New Materials by Mechanical Alloying Techniques, Calw-Hirsau, October 1988*, Deutsche Gesellschaft für Metallkunde, Informationsgesellschaft, Düsseldorf, 1989, pp. 79–84.
- 157 E. Gaffet and M. Harmelin, in A. R. Yavari and P. J. Desré (eds.), *Proc. Int. Symp. on Solid State Reaction, Grenoble, February 1990*, in *J. Phys., Coll. Phys. C4, Suppl. 14*, 51 (1990) 139–150.
- E. Gaffet and M. Harmelin, in F. H. Froes and J. J. deBarbadillo (eds.), *Proc. ASM Conf. on Structural Applications of Mechanical Alloying, Myrtle Beach, SC, March 26–29, 1990*, American Society for Metals, Metals Park, OH, 1990, p. 257.
- 158 M. Gerl and P. Guilmot, *Solid State Phenom.*, 3–4 (1988) 215–224.
- 159 B. M. Clemens and R. Sinclair, *Mater. Res. Soc. Bull.*, 15(2) (1990) 19.
- 160 K. Samwer, *Phys. Rep.*, 161(1) (1988) 1.
- 161 G. Martin and E. Gaffet, in A. R. Yavari and P. J. Desré (eds.), *Proc. Int. Symp. on Solid State Reaction, Grenoble, February 1990*, in *J. Phys., Coll. Phys. C4, Suppl. 14*, 51 (1990) 71–77.
- 162 F. H. Froes and J. J. deBarbadillo (eds.), *Proc. ASM Conf. on Structural Applications of Mechanical Alloying, Myrtle Beach, SC, March 26–29, 1990*, American Society for Metals, Metals Park, OH, 1990.
- 163 K. Lefki, P. Muret, N. Cherief and R. C. Cinti, *J. Appl. Phys.*, 69(1) (1991) 352–357.
- 164 N. Malhouroux, E. Gaffet and J. N. Patillon, *Proc. 3rd Int. Symp. on Trends and New Applications in Thin Films, (TATF91) Strasbourg, November 25–29, 1991*, pp. 35–37.
- 165 C. A. Dimitriadis, J. J. Werner, S. Logothetidis, M. Stutzman, J. Weber and R. Nesper, *J. Appl. Phys.*, 68(4) (1990) 1726–1734.
- 166 J. E. Mahan, K. M. Geib, G. Y. Robinson, R. G. Long, Y. Xinghua, G. Bai, M.-A. Nicolet and M. Nathan, *Appl. Phys. Lett.*, 56(21) (1990) 2126–2128.
- 167 C. A. Dimitriadis and J. H. Werner, *J. Appl. Phys.*, 68(1) (1990) 93–96.
- 168 K. M. Geib, J. E. Mahan, R. G. Long, M. Nathan and G. Bai, *J. Appl. Phys.*, 70(3) (1991) 1730–1736.
- 169 X. Wallart, H. S. Zeng, J. P. Nys and G. Dalmai, *Mater. Sci. Eng.*, B9 (1991) 253.
- 170 M. Michelini, F. Nava and E. Galli, *J. Mater. Res.*, 6(8) (1991) 1655–1663.
- 171 W. G. Moffatt, *The Handbook of Binary Phase Diagrams*, Vol. 3, Genium, New York, 1984.
- 172 M. J. Tenwick and H. A. Davies, *Int. J. Rapid Solid.*, 1 (1984–1985) 143–155.
- 173 R. Sinclair, *Mater. Trans., JIM*, 31(7) (1990) 628–635.
- 174 K. Holloway and R. Sinclair, *J. Appl. Phys.*, 61(4) (1987) 1359–1364.
- 175 W. Lur and L. J. Chen, *Appl. Phys. Lett.*, 54(13) (1989) 1217–1219.
- 176 K. Samwer, X. L. Yeh and W. L. Johnson, *J. Non-Cryst. Solids*, 61–62 (1984) 631–636.
- 177 T. Yamauchi, S. Zaima, K. Mizuno, H. Kitamura, Y. Koide and Y. Yasuda, *J. Appl. Phys.*, 69(10) (1991) 7050.